ABSTRACT

CHEN, JIAHAO. A Novel Fission Diffusion Synthetic Acceleration Method for Criticality Calculations. (Under the direction of Jia (Jason) Hou).

A wide selection of deterministic and stochastic methods have been developed to conduct nuclear reactor criticality calculations and to improve the efficiency of these methods, a branch of neutronics method research focuses on the acceleration of source convergence process which is solved with power iteration method. These acceleration schemes have a history almost as long as the deterministic methods themselves with different levels of versatility. With the increasing popularity of Monte Carlo methods, the so called hybrid neutronics methods have been introduced for the same purpose, though these hybrid neutronics methods, because of the characteristics of Monte Carlo methods on both theory and algorithmic levels, demonstrate unique performance and behaviors.

A novel Fission Diffusion Synthetic Acceleration (FDSA) method is proposed in this work for the acceleration of source convergence process in both deterministic and stochastic methods which utilize the power iteration method. This method is based on the previous work on a similar topic with further developments to improve the convergence stability and range of application. A multigroup one-dimensional derivation of the novel FDSA method is developed and numerically tested in both one-group and multigroup cases to prove its feasibility. Further, comparisons against contemporary acceleration methods are made, both theoretically and numerically, in order to better evaluate the performance of the novel FDSA method in the same cases.

Then, the FDSA method is then implemented in a hybrid neutronics solver with the intention to achieve source convergence acceleration and variance reduction in Monte Carlo simulations. As an extension to the numerical tests, a series of Monte Carlo simulations with continuous energy cross section are conducted using the hybrid solvers, the results of which demonstrate that the source convergence could be immediately attained with the FDSA feedback to the high

order transport calculations. The speedup in source convergence ranges from 10 to 20 times over the standalone Monte Carlo simulations for both a simple homogeneous slab and a complex C5G7 full core geometry, while the acceleration in power iterations by a factor of up to 10 can be achieved for deterministic methods. As for variance reduction, MC-FDSA is also competitive to MC-CMFD and is shown to reduce the real variance in fission source by up to 20%. Overall the proposed MC-FDSA method is proved to be successful in accelerating power iteration and source convergence acceleration, and reducing variance in Monte Carlo methods.

A Novel Fission Diffusion Synthetic Acceleration Method for Criticality Calculations

by
Jiahao Chen

A dissertation submitted to the Graduate Faculty of
North Carolina State University
in partial fulfillment of the
requirements for the Degree of
Doctor of Philosophy

Nuclear Engineering

Raleigh, North Carolina
2021

APPROVED BY:

Kostadin Ivanov	Dimitry Anistratov
Zhilin Li	Jia (Jason) Hou Chair of Advisory Committee

DEDICATION

To my family and friends.

BIOGRAPHY

The author Jiahao Chen was born in a small town in Hubei, China to his parents Wei Chen and Guirong Shen and has a sister Fang Chen. He went to Huazhong University of Science and Technology and received a bachelor's degree in Nuclear Engineering. After that he completed his master's degree in Nuclear Engineering at Shanghai Institute of Applied Physics, Chinese Academy of Science. In July 2017 he started his pursuance of a Doctor of Philosophy under the advisement of Dr. Jason Hou and Dr. Kostadin Ivanov.

ACKNOWLEDGEMENTS

This project is accomplished with advise and guidance from Dr. Jason Hou and Dr. Kostadin Ivanov. Without their consistent support and feedback I could not have completed this project.

I joined the Department of Nuclear Engineering at NC State as a graduate student in 2017 and have met so many inspiring and kind people. Without their friendship and companionship, I would not be able to finish this arduous journey, especially after the COVID-19 pandemic hit my hometown in Hubei and then again Raleigh, NC on this side of the planet. Although the months I lived in solitude in 2020 were the most productive period of the project, they were also the most depressing and inflictive in my life. For this I am truly grateful for your love and support during this turbulent time, through video chat and conversations.

I want to thank my classmates and friends Drs. Kaiyue Zeng, Yuchen Zhao and Yuchao Xu who are now professionals in their fields. Equal if not more gratitude to my fellow graduate students Yao Du, Da Cao, Kan Ni, Yuqing Huang, Joel Coale, William Dawn, Sandesh Bhaskar and Ghada Shkoukani who are soon to be doctors. I also want to express my appreciation to the former and current RDFMG group members, especially Dr. Paolo Balestra, Dr. Pascal Rouxelin and Mario Milev for their friendship and professional support. Throughout the graduate program I have learnt so much, through classes and professional advises, from my teachers and mentors. I want to thank Drs. Dmitriy Anistratov, Yousry Azmy and Zhilin Li for teaching me transport theory and mathematical methods, Dr. Maria Avramova for her kindness, and Dr. Robert Hayes for showing me what being an engineer means. Special gratefulness to Wade Chapman for the amazing summer time in Idaho.

Last but not least I want to thank my parents and my sister for their unconditional love and unrelenting encouragement across the globe and to my heart, and in turn I can only hope that I will match this by being your loving son and brother.

TABLE OF CONTENTS

LIST OF TABLES

LIST OF FIGURES

CHAPTER

1

INTRODUCTION

Criticality calculation has been the basis of reactor design since the first nuclear reactor built in Chicago during an experiment led by Enrico Fermi. Numerous theories and techniques have been discovered and investigated to solve the neutron transport equation, of which one of the main difficulties is the slow convergence of fission source due to past and current limitations of computational resources and numerical methods' efficiency. A branch of research on criticality calculation focuses on the improvement of efficiency and acceleration of said calculations. This includes the acceleration in deterministic methods that have been in use for decades and Monte Carlo (MC) methods that are winning popularity in recent years. The work presented here aims at accelerating the fission source convergence in both types of methods and introduces a novel Fission Diffusion Synthetic Acceleration (FDSA) method to accomplish this.

Monte Carlo (MC) methods have been used in a wider range of application of reactor design and analysis because of the versatility in detailed geometric modeling, utilization of continuous energy cross section data and simple parallelization. Compared to the deterministic methods, MC methods are generally considered as brute force methods as they require less approximations on multiple levels, MC methods tend to take up much more computational resources to reduce the inherent stochastic error. With the increasing amount of computing power and modern code algorithms, this issue has become less severe and the applications of MC methods have been made in areas such as cross section homogenization, burnup calculation and uncertainty quantification. However, the efficiency of MC methods still restricts the usage of MC methods in analysis of larger reactor systems. A branch of research on neutronics methods is dedicated to address this issue, in either accelerating the source convergence in skipped cycles or reduce the stochastic variance in active cycles or both. Similar to the acceleration methods in deterministic methods, hybrid MC-deterministic methods have been developed in a way that the solution to the low-order deterministic problem can be utilized to accelerate the high-order MC transport problem.

1.1 Iterative methods for neutronics calculation

In depicting the neutrons' transport in phase space, one would arrive at a transport equation with 7 dependencies for steady state situation, as shown in the following equation,

$$\begin{aligned} &\Omega \cdot \nabla \psi(\vec{r}, E, \Omega) + \Sigma_t(\vec{r}, E)\psi(\vec{r}, E, \Omega) = \\ &\int\int \Sigma_s(\vec{r}, \Omega' \cdot \Omega, E' \to E)\psi(\vec{r}, E', \Omega')d\Omega' dE' + \\ &\frac{1}{4\pi k}\int \nu\Sigma_f(\vec{r}, E' \to E)\int \psi(\vec{r}, E', \Omega')d\Omega' dE' \,, \end{aligned} \tag{1.1}$$

where $\Sigma_t(\vec{r},E), \Sigma_s(\vec{r},\Omega'\cdot\Omega,E'\rightarrow E)$ and $\nu\Sigma_f(\vec{r},E'\rightarrow E)$ are the cross section of nuclear reactions and $\psi(\vec{r},E,\Omega)$ is the angular neutron flux. The solution to this equation, i.e., the angular flux $\psi(\vec{r},E,\Omega)$, is dependent on angle, space and energy, and the high number of dimensions here prohibits the use of direct solvers for most scenarios. Iterative methods are widely used in solving problems derived from this equation for the benefits of faster convergence and requirement of less computational resources. Reactor criticality calculation is one of these derived problems which involves the multiplication factor, the ratio of the number of neutrons born in this generation against that of neutrons in the previous generation. The distribution of neutron flux, together with the multiplication factor, is important for designing reactors and nuclear waste management. Mathematically they are translated into the fundamental eigenvalue, or k_{eff} for a finite system, and the corresponding eigenvector. Thus the basis of criticality calculation is the power iteration method for both deterministic and MC methods. In the deterministic methods, a fixed source problem is solved in the inner iterations in the fashion of transport sweep to acquire the updated angular fluxes. These fluxes are then used to compute and update the scattering sources to continue the inner iterations. Once the inner iterations are converged, the eigenvalue is computed with the latest angular flux and the convergence is checked for the power iterations. This two-layer approach is widely applied in deterministic methods with different implementations to address the issue of high dimensional unknowns and solving for the eigenvalue efficiently. For physical problems with high dominance ratios, i.e., large second eigenvalue against the fundamental one, power iteration can only slowly converge the fission source and calls for the acceleration methods.

1.1.1 Acceleration methods for deterministic calculation

Iterative acceleration methods started from accelerating fixed source problem which is generally solved in inner iterations. Among the methods developed for this purpose, three received

intensive research interest, Quasi-Diffusion (QD), Coarse Mesh Finite Difference (CMFD), and Diffusion Synthetic Acceleration (DSA). To suit the need of accelerating power iteration, different forms of these methods were developed which are discussed in the following sections.

1.1.1.1 Acceleration methods for k-eigenvalue problem

The QD method [1, 2] is one of the nonlinear methods that utilize the diffusion-like low-order problem to accelerate high-order transport problem. Its essence lies in the evaluation of Eddington tensor, a nonlinear operator that extracts changes in shape of eigenvector to achieve rapid source convergence. For eigenvalue problem with normalization on neutron flux, this is quite beneficial in that the magnitude of eigenvector plays a much lesser role. Later QD was applied in the construction of multilevel methods in space and energy for advanced iterative schemes [3, 4].

The CMFD method [5] and later the partial current-based CMFD (pCMFD) [6] received increasing interest ever since its application in full-core Light Water Reactor (LWR) calculations. In a similar fashion to QD, CMFD updates the nonlinear diffusion operator with corrections evaluated using the high-order transport solution. After the success of application in LWR, CMFD gained enormous popularity in the nuclear engineering community and further developments have been extended to multilevel multigrid schemes [7–10], improved schemes with better convergence stability [11] and detailed comparison with other methods [12].

DSA started as a linear method for fixed source problems and one form of it was adapted for k-eigenvalue problem by Alcouffe [13, 14]. This form of DSA is somewhat similar to QD as the diffusive leakage terms are both corrected with transport information, albeit in different ways. A close examination mathematically and numerically [2] suggests that both DSA and QD have their advantages and drawbacks over each other. Recent developments on DSA, however, focuses more on fixed source problems [11, 15].

A specific form of DSA, or Fission Diffusion Synthetic Acceleration (FDSA), was proposed

by Urbatsch [16] and demonstrated with one-group cases along for both deterministic and hybrid MC calculations.

1.1.1.2 Previous work on FDSA

Urbatsch's form of FDSA [16] includes eigenvalue and fission source terms and bases the solvability condition with adjoint and forward diffusion solutions of the same eigenvalue problem. This provides rapid convergence rates for eigenvalue problems in which the flux distribution is diffusion-like. However, because the transport flux is normalized such that it's orthogonal to the adjoint diffusion flux, the performance of FDSA depends on the quality of said diffusion solutions. For cases where the flux is not so diffusion-like, the method's stability quickly deteriorates and requires damping, sometimes severe, of the correction terms to converge. Though options of different damping factors were tested, there seemed to be no rule for choosing one suitable for each case and the factors could only be chosen empirically by running repeated tests.

1.1.2 Monte Carlo methods for neutronics calculation

MC methods have the capabilities of modeling detailed geometry, utilizing continuous energy cross section data and high performance parallel computing, and have become one of the main computational tools for reactor design. To reach convergence with acceptable statistical errors with MC methods, vast amount of neutron history is required, and for problems with large optical thickness or loosely coupled fissionable regions, slow source convergence becomes the main obstacle in obtaining results efficiently. Further, because of the inherent statistical error in both flux and multiplication factor, it's not so easy to monitor the convergence process of MC methods on the fly.

To devise an indicator of source convergence process, researchers referred to information

theory based techniques [17, 18] for diagnostics of source convergence and dominance ratio calculations. The popular approach is the use of Shannon entropy in determining the convergence process of fission source [19]. In recent use of MC methods in criticality calculations, Shannon entropy is usually monitored together with the statistical error of the multiplication factor.

1.1.2.1 Hybrid Monte Carlo/Deterministic methods

With the diagnostic measures, MC calculations are still rather costly computationally compared to contemporary deterministic calculations. The development of hybrid MC/deterministic methods is aimed at this. Various techniques have been developed to accomplish either variance reduction [20–23] or acceleration of source convergence in MC methods. Most of these techniques involve the development of a hybrid MC/deterministic method which is structurally similar to the acceleration methods for deterministic methods, with MC transport calculation as high-order problem and the deterministic calculation as low-order problem. Within the scope of this project, we focus on the acceleration of source convergence with hybrid MC/deterministic method.

1.1.2.2 Source convergence acceleration

The research on source convergence acceleration in MC methods first targeted physical problems with large optical thickness regions where few neutrons would score[24]. The forward-based method utilizes the concept of neutron weight in MC method which was originally designed for tallying purposes. This was the first attempt to use QD to construct the low-order problem and to accelerate source convergence, and was further developed into functional MC method [25]. It has also been shown in simpler form that MC/QD method could achieve acceleration goals [26, 27].

With the feasibility of constructing hybrid methods in this manner proven, researchers also developed hybrid MC/CMFD[28–30] or MC/pCMFD [31] methods with different discretization

or implementation details, which was later generalized or functionalized [32–34]. It has also been shown that the stability of MC/CMFD method is similar to that of CMFD [35]. MC/CMFD was later coupled with thermal hydraulics feedback for multiphysics analysis [36].

OpenMC [37] is one of the recent developed MC/CMFD solvers. With CMFD acceleration capability for comparison purpose and open source access, it was chosen as the MC solver for the hybrid method we aimed to develop.

1.1.2.3 Variance reduction

Another main feature of the hybrid neutronics methods is the variance reduction in the active cycles, mainly to reduce the inherent statistical error in MC methods. Like how the acceleration of source convergence is achieved in the inactive cycles, variance reduction is also realized by applying a certain importance function on the source particles' distribution. Successes were made with the Consistent Adjoint Driven Importance Sampling (CADIS) [21, 38] which computes the adjoint eigenfunction as the improved source distribution, and the Response Matrix method [22, 39] that constructs a response matrix and achieves variance reduction with its response. Although the actual application in the active cycles is not that different from the one in inactive cycles, early work on MC-CMFD showed that the hybrid methods can lower the magnitude of variance by a factor of up to 10 [32, 40] by applying the CMFD feedback in multigroup cases. More recently, Park et al [41] extended MC-CMFD to continuous energy MC method, and found out that the variance reduction with MC-CMFD could also be observed in full core calculation with continuous energy cross section, although the reduction is only 50% less than the standalone MC simulation.

1.2 Motivation of FDSA

In searching for an acceleration scheme with rapid convergence rate and solid stability for the hybrid method, one would find that DSA is a good candidate. The application of DSA in hybrid neutronics method is absent and previous work of FDSA yielded compromised results with impacted convergence stability. In fact, even with the one-group slab-geometry case [16], the FDSA method was not able to meet the expectation, and was certainly not comparable to later methods such as CMFD.

This led to our preliminary study on MC-DSA [42], the results of which are included in Appendix-B.1. The effort to use DSA for acceleration of eigenvalue problem was not satisfying, either. For the simple homogeneous slab problem, the MC-DSA solver we constructed had trouble in providing rapid convergence rate and the low-order DSA feedback needed to be turned off after certain iterations to produce adequate acceleration effect. The convergence behavior, like what was observed on FDSA, was not stable and required careful manipulation of the calculation configuration. The reason behind this behavior was thought to be the lack of fission synthetic operators to capture the changes of eigenstates between MC cycles.

With the realization that the inclusion of fission source is unavoidable, we turned to develop such a method and made several improvements on the original FDSA method, including skipping the preconditioning with forward and adjoint diffusion solutions, simplifying the between-iteration steps, and discarding damping on correction terms. These changes were made in the hope that the novel FDSA method would display a stable convergence behavior and superior convergence rate at the same time. Further, with the success of such a method, the development of both multilevel deterministic method and hybrid MC-FDSA method would be made feasible, which would ideally possess the source convergence acceleration and variance reduction features.

With these concepts and goals in mind, we will continue to the introduction of the novel

FDSA method in the following chapter.

CHAPTER

2

THEORY

This chapter features the theoretical formulation, discretization and implementation of the FDSA method. In pursuit of an acceleration method for k-eigenvalue problems, we formulated and developed the novel multigroup FDSA scheme based on the previous work by Urbastch [16]. However, a different approach is taken to address the non-linearity in the k-eigenvalue problems with power normalizations as this new FDSA method requires no preconditioning with adjoint and forward diffusion solution which originates from the same transport problem. This significantly simplified the FDSA scheme and reduced its complexity to the same level of the original DSA method applied in fixed source problems.

2.1 Monte Carlo eigenvalue simulations

The increasing use of MC method to solve eigenvalue problems for nuclear reactor analysis is rooted in its ability to characterize detailed geometric modeling and use of continuous energy nuclear data, a process that could potentially circumvent multiple approximations made in conventional group constant generation approaches.

The general process of Monte Carlo neutronics methods includes four steps:

1. Particle sampling: individual particles are sampled with the random seed generator based on either a user-defined source distribution at the beginning of the simulation or an updated distribution from the previous cycle.

2. Transport process: each particle the undergoes the simulation of the transport process based on the physical modeling. Each particle's track, direction, speed and reaction types are recorded and counted towards the tallies. Particles that undergo a fission process are also stored into the fission bank for the next cycle.

3. Tallies and post-processing: once all particles have been simulated and accounted for, the post-processing steps begin and the information from these particles is gathered, including their locations in space, energy, the times of different reactions that these particles have gone through in this cycle. The information is then folded into the eigenvalues and the user-defined tallies that represent the physical variables needed for analysis.

4. Updating probability density function (PDF): after the post-processing steps are completed, the default tallies on fission source distribution are then used to update the probability density function and to get ready for the next Monte Carlo cycle. Another way to finish this step is to store all fission neutrons from the previous cycle and to start the next cycle with them, thus skipping the sampling process.

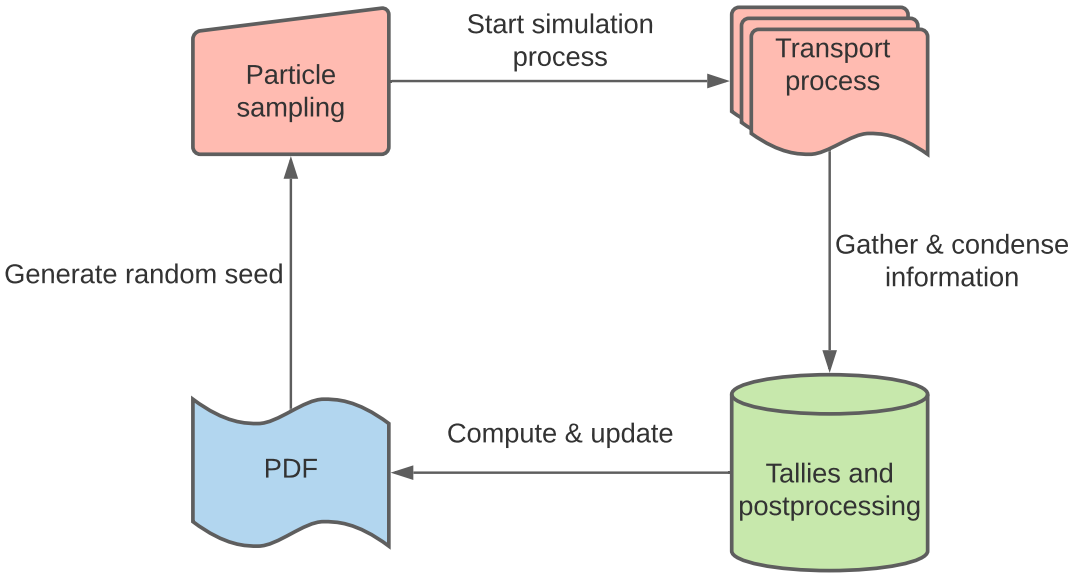

Figure 2.1: General process of Monte Carlo methods.

The versatility of Monte Carlo methods wins over the support of researchers and industry users in the applications of reactor analysis, especially criticality calculation. However, two main issues arise in the use of MC method, mainly how to determine the convergence of MC simulation and how to quantify the statistical error in the results gathered in active cycles. These two issues are addressed by the use of Shannon entropy and different variances respectively.

2.1.1 Shannon entropy

Because the convergence process in MC method is significantly impacted by the fluctuation caused by statistical error, applying a hard check on either eigenvalue or other values of interest might not be ideal and one could more easily encounter a false convergence. Further, only monitoring the eigenvalue's evolution from cycle to cycle does not guarantee the convergence of local quantities such as flux or fission source, especially in cases with high dominance ratio

or highly diffusion domain. Directly checking the flux or fission source would require a spatial mesh and since no reference solution might be known and without any knowledge about the magnitude of statistical error, one would find it difficult to correctly evaluate the convergence process. Brown et al [19] applied the Shannon entropy, an estimation of a system's state of randomness from the information science, to the MC fission source distribution and showed that it could characterize the fission source's convergence stabilizing as more MC cycles are completed.

The computation of Shannon entropy requires a spatial mesh that encapsulates all fission sources in the physical problem. Thus the fission source within cell i could be evaluated as

$$S_i = \frac{\text{Number of fission sources inside cell } i}{\text{Total number of fission sources in all cells}}, \tag{2.1}$$

and the Shannon entropy is defined as

$$H_{src} = -\sum_{i=1}^{I} S_i \log_2 S_i. \tag{2.2}$$

Because the fission sources S_i are normalized such that their sum is 1, the Shannon entropy is always positive but its value depends on the spatial mesh.

2.1.2 Variances of sampled variables

2.1.2.1 Variance of the mean

In MC tallies, the variance of a sample is used to determine the confidence interval of variables of interest and different techniques have been developed to provide correct evaluations of variances. The commonly used form of variance is the variance of the mean.

Suppose that we have a pool of samples of variable X_i, and the mean value of them as $\bar{X}$. The variance of the mean is, by the Bienaymé formula,

$$Var(\bar{X}) = Var\left(\frac{1}{N}\sum_{i=1}^{I} X_i\right) = \frac{1}{N^2}(\sum_{i=1}^{N} Var(X_i)) = \frac{1}{N^2}(N\sigma^2) = \frac{\sigma^2}{N}. \tag{2.3}$$

The variance σ^2 of samples X_i, modified with Bessel's correction, is

$$\sigma^2 = \frac{1}{N-1}\sum_{i=1}^{N}(X_i - \bar{X})^2 = \frac{1}{N-1}\left(\sum_{i-1}^{N} X_i^2 - N\bar{X}^2\right). \tag{2.4}$$

So the variance of the mean $\sigma_{\bar{X}}^2$ is

$$\sigma_{\bar{X}}^2 = \frac{1}{N-1}\left(\frac{1}{N}\sum_{i-1}^{N} X_i^2 - \bar{X}^2\right). \tag{2.5}$$

This form of variance of the mean is suitable for MC simulations as only two sets of sample data X_i and $\bar{X}$ need to be saved in memory and the variance of the mean could be calculated at each cycle as the simulation marches on.

2.1.2.2 Apparent and real variances

As researchers start to focus on the local properties of variables in MC simulations, it was found that the true variance of such properties could be significantly larger than the variance of the mean presented above [43]. Ueki [44] suggested the use of real variance against apparent variance to represent the true variance of variables in MC and Shim and Kim [45] later provided an alternative form of such definitions.

In order to evaluate the apparent and real variance of a variable X, one would need to repeat the same simulation M times and acquire M sets of the variable's mean value X_m and variance σ_m^2. The apparent variance is simply the mean of the variance

$$\sigma_A^2 = \frac{1}{M}\sum_{m=1}^{M}\sigma_m^2, \tag{2.6}$$

while the real variance is defined as the variance of the mean value X_m

$$\sigma_R^2 = \frac{M}{M-1}\left(\frac{1}{M}\sum_{m=1}^{M} X_m^2 - \left[\frac{1}{M}\sum_{m=1}^{M} X_m\right]^2\right). \tag{2.7}$$

The apparent variance characterizes how the interval of confidence changes on the repeated runs of the same case, while the real variance estimates the behavior of the mean values. Previous work [30, 32, 41, 46] has shown that the real variance of local properties of interest, such as flux and fission rate in fuel pins, could be much higher than the apparent variance for MC solvers, in either multigroup or continuous energy simulations. Thus these two estimators have been widely applied to assess the performance of hybrid neutronics method in the aspect of variance reduction. The real-to-apparent ratio $r_{R/A} = \frac{\sigma_R}{\sigma_A}$ serves as a more direct way to look at the reduction from the apparent variance to the real one.

2.2 Formulation of FDSA method

The formulation and discretization of multigroup FDSA method is presented here, together with a finite volume scheme for multidimensional applications. A one-speed formulation of the same method could be found in Appendix-A.1.

2.2.1 Multigroup formulation of FDSA

Consider the multi-group transport equation for k-eigenvalue problem in a slab geometry with $x \in [0, X]$,

$$\mu\frac{\partial \psi_g(x,\mu)}{\partial x} + \Sigma_{t,g}(x)\psi_g(x,\mu) = \frac{1}{2}\sum_{g'=1}^{G}\Sigma_{s,g'\to g}(x)\int_{-1}^{1}\psi_{g'}(x,\mu)d\mu + \frac{1}{2k}\chi_g(x)\sum_{g'=1}^{G}\nu_{f,g'}\Sigma_{f,g'}(x)\int_{-1}^{1}\psi_{g'}(x,\mu)d\mu\ . \tag{2.8}$$

Let $\phi_g = \int_{-1}^{1} \psi_g d\mu$ and omit the dependencies and add indices for iterations:

$$\mu \frac{\partial \psi_g^{(l+1/2)}}{\partial x} + \Sigma_{t,g} \psi_g^{(l+1/2)} = \frac{1}{2} \sum_{g'=1}^{G} \Sigma_{s,g' \to g} \phi_{g'}^{(l)} + \frac{\chi_g}{2k^{(l)}} \sum_{g'=1}^{G} \nu_{f,g'} \Sigma_{f,g'} \phi_{g'}^{(l)} \ , \tag{2.9}$$

where l denotes the iteration index and g for a total of G energy groups.

For transport calculation we equate $\psi_g^{(l+1)} = \psi_g^{(l+1/2)}$ and move to the next iteration. In the acceleration scheme we define the correction term as

$$p^{(l+1)} = \psi_g - \psi_g^{(l+1/2)} \ , \tag{2.10}$$

where ψ is the true solution to the transport equation, and the intermediate step is completed with

$$\psi_g^{(l+1)} = \psi_g^{(l+1/2)} + p_g^{(l+1)} \ . \tag{2.11}$$

Replace the true solution ψ and ϕ in Eq. (2.8) with Eq. (2.10)

$$\begin{aligned} \mu \frac{\partial \left(\psi_g^{(l+1/2)} + p_g^{(l+1)} \right)}{\partial x} + \Sigma_{t,g} \left(\psi_g^{(l+1/2)} + p_g^{(l+1)} \right) = \\ \frac{1}{2} \sum_{g'=1}^{G} \Sigma_{s,g' \to g} \phi_{g'}^{(l+1/2)} + \frac{\chi_g}{2k^{(l)}} \sum_{g'=1}^{G} \nu_{f,g'} \Sigma_{f,g'} \left(\phi_{g'}^{(l+1/2)} + \int_{-1}^{1} p_{g'}^{(l+1)} d\mu \right) \ . \end{aligned} \tag{2.12}$$

Subtract Eq. (2.9) from Eq. (2.12) and rearrange

$$\begin{aligned} \mu \frac{\partial p_g^{(l+1)}}{\partial x} + \Sigma_{t,g} p_g^{(l+1)} - \frac{1}{2} \sum_{g'=1}^{G} \Sigma_{s,g' \to g} \int_{-1}^{1} p_{g'}^{(l+1)} d\mu - \frac{\chi_g}{2k} \sum_{g'=1}^{G} \nu_{f,g'} \Sigma_{f,g'} \int_{-1}^{1} p_{g'}^{(l+1)} d\mu = \\ \frac{\chi_g}{2k} \sum_{g'=1}^{G} \nu_{f,g'} \Sigma_{f,g'} \phi_{g'}^{(l+1/2)} - \frac{\chi_g}{2k^{(l)}} \sum_{g'=1}^{G} \nu_{f,g'} \Sigma_{f,g'} \phi_{g'}^{(l)} \ . \end{aligned} \tag{2.13}$$

Define the correction terms on scalar flux and current

$$f_{0,g}^{(l+1)} = \int_{-1}^{1} p_g^{(l+1)} d\mu \ , \tag{2.14}$$

$$f_{1,g}^{(l+1)} = \int_{-1}^{1} \mu p_g^{(l+1)} d\mu \ , \tag{2.15}$$

and substitute $\int_{-1}^{1} p_g^{(l+1)} d\mu$ in the previous equation:

$$\mu \frac{\partial p_g^{(l+1)}}{\partial x} + \Sigma_{t,g} p_g^{(l+1)} - \frac{1}{2} \sum_{g'=1}^{G} \Sigma_{s,g'\to g} f_{0,g'}^{(l+1)} - \frac{\chi_g}{2k} \sum_{g'=1}^{G} \nu_{f,g'} \Sigma_{f,g'} f_{0,g'}^{(l+1)} = \frac{\chi_g}{2k} \sum_{g'=1}^{G} \nu_{f,g'} \Sigma_{f,g'} \phi_{g'}^{(l+1/2)} - \frac{\chi_g}{2k^{(l)}} \sum_{g'=1}^{G} \nu_{f,g'} \Sigma_{f,g'} \phi_{g'}^{(l)} \ . \tag{2.16}$$

Apply operator $\int_{-1}^{1} \cdot d\mu$ on Eq. (2.16):

$$\frac{\partial f_{1,g}^{(l+1)}}{\partial x} + \Sigma_{t,g} f_{0,g}^{(l+1)} - \sum_{g'=1}^{G} \Sigma_{s,g'\to g} f_{0,g'}^{(l+1)} - \frac{\chi_g}{k} \sum_{g'=1}^{G} \nu_{f,g'} \Sigma_{f,g'} f_{0,g'}^{(l+1)} = \frac{\chi_g}{k} \sum_{g'=1}^{G} \nu_{f,g'} \Sigma_{f,g'} \phi_{g'}^{(l+1/2)} - \frac{\chi_g}{k^{(l)}} \sum_{g'=1}^{G} \nu_{f,g'} \Sigma_{f,g'} \phi_{g'}^{(l)} \ . \tag{2.17}$$

Apply operator $\int_{-1}^{1} \mu \cdot d\mu$ on Eq. (2.16):

$$\frac{\partial}{\partial x} \int_{-1}^{1} \mu^2 p_g^{(l+1)} d\mu + \Sigma_{t,g} f_{1,g}^{(l+1)} = 0 \ . \tag{2.18}$$

Apply the P_1 approximation on the correction term $p_g^{(l+1/2)}$

$$p_g^{(l+1)} \approx \frac{1}{2} \left(f_{0,g}^{(l+1)} + 3\mu f_{1,g}^{(l+1)} \right) \ , \tag{2.19}$$

and substitute in Eq. (2.18):

$$f_{1,g}^{(l+1)} = -\frac{1}{3\Sigma_{t,g}} \frac{\partial}{\partial x} f_{0,g}^{(l+1)} \ . \tag{2.20}$$

Substitute Eq. (2.20) into Eq. (2.17), and we have:

$$-\frac{\partial}{\partial x}\frac{1}{3\Sigma_{t,g}}\frac{\partial}{\partial x} f_{0,g}^{(l+1)} + \Sigma_{t,g} f_{0,g}^{(l+1)} - \sum_{g'=1}^{G} \Sigma_{s,g'\to g} f_{0,g'}^{(l+1)} - \frac{\chi_g}{k} \sum_{g'=1}^{G} \nu_{f,g'} \Sigma_{f,g'} f_{0,g'}^{(l+1)} = \frac{\chi_g}{k} \sum_{g'=1}^{G} \nu_{f,g'} \Sigma_{f,g'} \phi_{g'}^{(l+1/2)} - \frac{\chi_g}{k^{(l)}} \sum_{g'=1}^{G} \nu_{f,g'} \Sigma_{f,g'} \phi_{g'}^{(l)} \ . \tag{2.21}$$

Replacing the true eigenvalue k on the left hand said with the eigenvalue from the latest transport calculation $k^{(l+1/2)}$, we would arrive at

$$-\frac{\partial}{\partial x}\frac{1}{3\Sigma_{t,g}}\frac{\partial}{\partial x} f_{0,g}^{(l+1)} + \Sigma_{t,g} f_{0,g}^{(l+1)} - \sum_{g'=1}^{G} \Sigma_{s,g'\to g} f_{0,g'}^{(l+1)} - \frac{\chi_g}{k^{(l+1/2)}} \sum_{g'=1}^{G} \nu_{f,g'} \Sigma_{f,g'} f_{0,g'}^{(l+1)} = \frac{\chi_g}{k^{(l+1/2)}} \sum_{g'=1}^{G} \nu_{f,g'} \Sigma_{f,g'} \phi_{g'}^{(l+1/2)} - \frac{\chi_g}{k^{(l)}} \sum_{g'=1}^{G} \nu_{f,g'} \Sigma_{f,g'} \phi_{g'}^{(l)} \ . \tag{2.22}$$

The correction term $f_0^{(l+1/2)}$ can be acquired by solving Eq. (B.1), and is applied to scalar flux by

$$\phi_g^{(l+1)} = \phi_g^{(l+1/2)} + f_{0,g}^{(l+1)} \ , \tag{2.23}$$

and the new eigenvalue is evaluated with

$$k^{(l+1)} = k^{(l+1/2)} \frac{\sum_{g'=1}^{G} \int \nu_{g'} \Sigma_{f,g'} \phi_{g'}^{(l+1)} dx}{\sum_{g'=1}^{G} \int \nu_{g'} \Sigma_{f,g'} \phi_{g'}^{(l+1/2)} dx} \ , \tag{2.24}$$

where $k^{(l+1/2)}$ is the eigenvalue from the latest transport sweep, or

$$k^{(l+1)} = \frac{\sum_{g'=1}^{G} \int \nu_{g'} \Sigma_{f,g'} \phi_{g'}^{(l+1)} dx}{\sum_{g'=1}^{G} J_{g'}(x=X) + \sum_{g'=1}^{G} J_{g'}(x=J) + \sum_{g'=1}^{G} \int \Sigma_{a,g'} \phi_{g'}^{(l+1/2)} dx} \ . \tag{2.25}$$

2.2.2 Discretization of multigroup FDSA equation

Consider a slab of width L with a mesh of J cells. With a S_N angular quadrature set, the discrete transport equation is

$$\frac{\mu_m}{h_j}\left(\psi_{m,g,j+1/2}-\psi_{m,g,j-1/2}\right)+\Sigma_{t,g,j}\psi_{m,g,j}-\frac{1}{2}\sum_{g'=1}^{G}\Sigma_{s,g'\to g,j}\phi_{g',j}=\frac{\chi_g}{2k}\sum_{g'=1}^{G}\nu_{f,g',j}\Sigma_{f,g',j}\phi_{g',j}, \tag{2.26}$$

where ψ is the true solution and $\phi_{g,j}=\sum_{m=1}^{N}\psi_{m,g,j}\omega_m$, and the angular quadrature weights are such that $\sum_{m=1}^{N}\omega_m=2$. The indexes j and $j\pm 1/2$ denote the cell-center and cell-edge quantities respectively. With Diamond Differencing we have:

$$\psi_{m,g,j}=\frac{1}{2}\left(\psi_{m,g,j+1/2}+\psi_{m,g,j-1/2}\right). \tag{2.27}$$

The right boundary is reflective and the left boundary is vacuum:

$$\begin{aligned}\psi_{m,g,1/2}&=\psi_{n,g,1/2}, & \mu_m&=-\mu_n>0,\\ \psi_{m,g,J+1/2}&=0, & \mu_m&<0,\end{aligned} \tag{2.28}$$

The iterative form of the transport equation, Eq. (2.26) is

$$\begin{aligned}&\frac{\mu_m}{h_j}\left(\psi^{(l+1/2)}_{m,g,j+1/2}-\psi^{(l+1/2)}_{m,g,j-1/2}\right)+\Sigma_{t,g,j}\psi^{(l+1/2)}_{m,g,j}=\\ &\frac{1}{2}\sum_{g'=1}^{G}\Sigma_{s,g'\to g,j}\phi^{(l)}_{g',j}+\frac{\chi_g}{2k^{(l)}}\sum_{g'=1}^{G}\nu_{f,g',j}\Sigma_{f,g',j}\phi^{(l)}_{g',j},\end{aligned} \tag{2.29}$$

$$\psi^{(l+1/2)}_{m,g,j}=\frac{1}{2}\left(\psi^{(l+1/2)}_{m,g,j+1/2}+\psi^{(l+1/2)}_{m,g,j-1/2}\right), \tag{2.30}$$

where l indicates the iteration. The correction terms on the angular flux are defined as:

$$p_{m,g,j}^{(l+1)} = \psi_{m,g,j} - \psi_{m,g,j}^{(l+1/2)}, \tag{2.31}$$

$$p_{m,g,j\pm1/2}^{(l+1)} = \psi_{m,g,j\pm1/2} - \psi_{m,g,j\pm1/2}^{(l+1/2)}, \tag{2.32}$$

and we also have the Diamond Difference relationship and definition of correction on the scalar flux ϕ

$$p_{m,g,j}^{(l+1)} = \frac{1}{2}\left(p_{m,g,j+1/2}^{(l+1)} + p_{m,g,j-1/2}^{(l+1)}\right), \tag{2.33}$$

$$\phi_{g,j} = \phi_{g,j}^{(l+1/2)} + \sum_{m=1}^{N} p_{m,g,j}^{(l+1)} \tag{2.34}$$

Subtract Eq. (2.29) from Eq. (2.26) and replace corresponding terms in Eq. (2.31), we would arrive at

$$\frac{\mu_m}{h_j}\left(p_{m,g,j+1/2}^{(l+1)} - p_{m,g,j-1/2}^{(l+1)}\right) + \Sigma_{t,g,j} p_{m,g,j}^{(l+1)} - \frac{1}{2}\sum_{g'=1}^{G}\Sigma_{s,g'\to g,j}\sum_{m=1}^{N} p_j^{(l+1)} = \frac{\chi_g}{2k}\sum_{g'=1}^{G}\nu_{f,g',j}\Sigma_{f,g',j}\phi_{g',j} - \frac{\chi_g}{2k^{(l)}}\sum_{g'=1}^{G}\nu_{f,g',j}\Sigma_{f,g',j}\phi_{g',j}^{(l)}, \tag{2.35}$$

Add and subtract $\frac{\chi_g}{2k}\sum_{g'=1}^{G}\nu_{f,g',j}\Sigma_{f,g',j}\phi_{g',j}^{(l+1/2)}$ on the right hand side of Eq. (2.35), we have:

$$\frac{\mu_m}{h_j}\left(p_{m,g,j+1/2}^{(l+1)} - p_{m,g,j-1/2}^{(l+1)}\right) + \Sigma_{t,g,j} p_{m,g,j}^{(l+1)} - \frac{1}{2}\sum_{g'=1}^{G}\Sigma_{s,g'\to g,j}\sum_{m=1}^{N} p_j^{(l+1)} = \frac{\chi_g}{2k}\sum_{g'=1}^{G}\nu_{f,g',j}\Sigma_{f,g',j}\phi_{g',j}^{(l+1/2)} - \frac{\chi_g}{2k^{(l)}}\sum_{g'=1}^{G}\nu_{f,g',j}\Sigma_{f,g',j}\phi_{g',j}^{(l)} + \frac{\chi_g}{2k}\sum_{g'=1}^{G}\nu_{f,g',j}\Sigma_{f,g',j}\phi_{g',j} - \frac{\chi_g}{2k}\sum_{g'=1}^{G}\nu_{f,g',j}\Sigma_{f,g',j}\phi_{g',j}^{(l+1/2)}. \tag{2.36}$$

Replace the last two terms with $\frac{\chi_g}{2k}\sum_{g'=1}^{G}\nu_{f,g',j}\Sigma_{f,g',j}\sum_{m=1}^{N}p_{m,g',j}^{(l+1)}$ and rearrange, we have:

$$\frac{\mu_m}{h_j}\left(p_{m,g,j+1/2}^{(l+1)}-p_{m,g,j-1/2}^{(l+1)}\right)+\Sigma_{t,g,j}p_{m,g,j}^{(l+1)} - \frac{\chi_g}{2k}\sum_{g'=1}^{G}\nu_{f,g',j}\Sigma_{f,g',j}\sum_{m=1}^{N}p_{m,g',j}^{(l+1)}-\frac{1}{2}\sum_{g'=1}^{G}\Sigma_{s,g'\to g,j}\sum_{m=1}^{N}p_{j}^{(l+1)} = \frac{\chi_g}{2k}\sum_{g'=1}^{G}\nu_{f,g',j}\Sigma_{f,g',j}\phi_{g',j}^{(l+1/2)}-\frac{\chi_g}{2k^{(l)}}\sum_{g'=1}^{G}\nu_{f,g',j}\Sigma_{f,g',j}\phi_{g',j}^{(l)}\,. \quad (2.37)$$

Add and subtract $\frac{1}{2}\sum_{g'=1}^{G}\Sigma_{s,g'\to g,j}\phi_{g',j}^{(l+1/2)}$ on the right hand side of Eq. (2.37), we have:

$$\frac{\mu_m}{h_j}\left(p_{m,g,j+1/2}^{(l+1)}-p_{m,g,j-1/2}^{(l+1)}\right)+\Sigma_{t,g,j}p_{m,g,j}^{(l+1)} - \frac{\chi_g}{2k}\sum_{g'=1}^{G}\nu_{f,g',j}\Sigma_{f,g',j}\sum_{m=1}^{N}p_{m,g',j}^{(l+1)}-\frac{1}{2}\sum_{g'=1}^{G}\Sigma_{s,g'\to g,j}\sum_{m=1}^{N}p_{j}^{(l+1)} = \frac{\chi_g}{2k}\sum_{g'=1}^{G}\nu_{f,g',j}\Sigma_{f,g',j}\phi_{g',j}^{(l+1/2)}-\frac{\chi_g}{2k^{(l)}}\sum_{g'=1}^{G}\nu_{f,g',j}\Sigma_{f,g',j}\phi_{g',j}^{(l)}\,. \quad (2.38)$$

The boundary conditions become:

$$\begin{aligned} p_{m,g,1/2}^{(l+1)} &= p_{n,g,1/2}^{(l+1)}, & \mu_m &= -\mu_n > 0, \\ p_{m,g,j+1/2}^{(l+1)} &= 0, & \mu_m &< 0, \end{aligned} \quad (2.39)$$

Eq. (2.37) is exact but just as difficult to solve as the original transport equation, so we proceed to derive the diffusion-like form of it.

Define the angular moments of correction terms:

$$f_{0,g,j}^{(l+1)} = \sum_{m=1}^{N}p_{m,g,j}^{(l+1)}\omega_m, \quad (2.40)$$

$$f_{1,g,j}^{(l+1)} = \sum_{m=1}^{N}\mu_m p_{m,g,j}^{(l+1)}\omega_m, \quad (2.41)$$

Apply an operator $\sum_{m=1}^{N}(\cdot)\,\omega_m$ on Eq. (2.37) and plug in Eq. (2.40) and Eq. (2.41), we have

$$\frac{1}{h_j}\left(f_{1,g,j+1/2}^{(l+1)}-f_{1,g,j-1/2}^{(l+1)}\right)+\Sigma_{t,g,j}f_{0,g,j}^{(l+1)}-\sum_{g'=1}^{G}\Sigma_{s,g'\to g,j}f_{0,g',j}^{(l+1)}-\frac{\chi_g}{k}\sum_{g'=1}^{G}\nu_{f,g',j}\Sigma_{f,g',j}f_{0,g,j}^{(l+1)}=$$
$$\frac{\chi_g}{k}\sum_{g'=1}^{G}\nu_{f,g',j}\Sigma_{f,g',j}\phi_{g',j}^{(l+1/2)}-\frac{\chi_g}{k^{(l)}}\sum_{g'=1}^{G}\nu_{f,g',j}\Sigma_{f,g',j}\phi_{g',j}^{(l)}\,,1\le j\le J. \quad (2.42)$$

Apply another operator $\sum_{m=1}^{N}\mu_m(\cdot)\,\omega_m$ on Eq. (2.37) and plug in Eq. (2.40) and Eq. (2.41), we have

$$\frac{1}{3h_j}\left(f_{0,g,j+1/2}^{(l+1)}-f_{0,g,j-1/2}^{(l+1)}\right)+\Sigma_{t,g,j}f_{1,g,j}^{(l+1)}=0,1\le j\le J. \quad (2.43)$$

Applying the same operators on Eq. (2.33) yields

$$f_{0,g,j}^{(l+1)}=\frac{1}{2}\left(f_{0,g,j+1/2}^{(l+1)}+f_{0,g,j-1/2}^{(l+1)}\right), \quad (2.44)$$
$$f_{1,g,j}^{(l+1)}=\frac{1}{2}\left(f_{1,g,j+1/2}^{(l+1)}+f_{1,g,j-1/2}^{(l+1)}\right). \quad (2.45)$$

Assuming the angular flux correction is linearly anisotropic,

$$p_{m,g,j}^{(l+1)}\approx\frac{1}{2}\left(f_{0,g,j}^{(l+1)}+3\mu_n f_{1,g,j}^{(l+1)}\right), \quad (2.46)$$

the vacuum boundary on the right side, represented by zero incoming partial current, would be

$$\begin{aligned}0&=\sum_{\mu_m<0}\mu_m p_{m,g,j+1/2}^{(l+1)}\omega_m\\&\approx\sum_{\mu_m<0}\frac{1}{2}\mu_m\left(f_{0,g,J+1/2}^{(l+1)}+3\mu_n f_{1,g,J+1/2}^{(l+1)}\right)\omega_m\\&=\frac{1}{2}\sum_{\mu_m<0}\mu_m\omega_m f_{0,g,J+1/2}^{(l+1)}+\frac{3}{2}\sum_{\mu_m<0}\mu_m^2\omega_m f_{1,g,J+1/2}^{(l+1)}\,.\end{aligned} \quad (2.47)$$

Let $\gamma = 2\sum_{\mu_m>0}\mu_m\omega_m$ and we also have

$$\sum_{\mu_m<0}\mu_m^2\omega_m = \frac{1}{2}\sum_{m=1}^{N}\mu_m^2\omega_m = \frac{1}{3}\,. \tag{2.48}$$

The right boundary condition becomes

$$0 = -\gamma f_{0,g,J+1/2}^{(l+1)} + 2f_{1,g,J+1/2}^{(l+1)}\,. \tag{2.49}$$

The left boundary condition is simply

$$f_{1,g,1/2}^{(l+1)} = 0\,. \tag{2.50}$$

To achieve consistent discretization in the low-order problem, we need to eliminate $f_{0,g,j}^{(l+1)}$ and $f_{1,g,j}^{(l+1)}$ in Eq. (2.42) and Eq. (2.43) with Eq. (2.44) and Eq. (2.45). However, because of the scattering and fission term on the RHS in Eq. (2.42), this procedure would yield a rather complicate system of equations. Thus we apply the diffusion approximation on the current correction instead

$$f_{1,g,j+1/2}^{(l+1)} = -\frac{2}{3}\left(\frac{f_{0,g,j+1}^{(l+1)} - f_{0,g,j}^{(l+1)}}{\Sigma_{t,g,j+1}h_{j+1} + \Sigma_{t,g,j}h_j}\right), 1 \le j \le J-1\,, \tag{2.51}$$

Thus we arrive at a system of equations comprised of Equations (2.42), (2.49) and (2.50). The elimination of the current correction $f_{1,g,j\pm1/2}^{(l+1)}$ in Eq. (2.42) would yield a diagonal dominant matrix which then could be solved for the flux correction $f_{0,g,j}^{(l+1)}$. The cost of using cell-average discretization instead of cell-edge discretization will likely be the deterioration of convergence stability to some extent, according to previous research[12].

Here are some observations on the FDSA low-order equation, Eq. (2.42):

1. The inclusion of eigenvalues from transport calculation, $k^{(l)}$ and $k^{(l+1/2)}$, makes the low-order problem nonlinear. Relating to the linear behavior of DSA method, this nonlinear feature seems to be adapting to the eigenvalue problem for which the FDSA method is intended.

2. The scattering and fission terms on the left hand side, $\sum_{g'=1}^{G} \Sigma_{s,g'\to g} f_{0,g'}^{(l+1)}$ and $\sum_{g'=1}^{G} \nu_{f,g'} \Sigma_{f,g'} f_{0,g'}^{(l+1)}$, indicates that even though the system of equations of Eq. (B.1), if written in matrix form, is still diagonal dominant, there will be more stripes parallel to the diagonal no matter how it is discretized. This is more complicated and difficult to solve than the contemporary methods such as CMFD and QD, and becomes exceedingly so with increasing number of energy groups one intends to use in the low-order problem.

3. The low-order problem itself is not an eigenvalue problem. According to Adams and Larsen [2], eigenvalue problems are more “naturally" accelerated with low-order problems constructed as eigenvalue problems themselves. What this indicates for the FDSA method is not clear, however, Eq. (B.1) only needs to be solved once between consecutive transport calculations. On this aspect it seems that even though it’s more complex than other methods as more terms are involved, solving Eq. (B.1) might not be as burdensome as we thought.

For implementation in a multidimensional code, the finite volume discretization scheme could be acquired by the following procedure. The space notation is $(x,y,z) \to i,j,k$, energy group $g',g \in (1,G)$ and volume-integral inner product $\left\langle \cdot \right\rangle$. The cross section and scalar flux are defined as

$$\overline{\Sigma}^{g}_{t,i,j,k} = \frac{\left\langle \Sigma^{g}_{t,i,j,k} \phi^{g}_{i,j,k} \right\rangle}{\left\langle \phi^{g}_{i,j,k} \right\rangle}, \tag{2.52a}$$

$$\overline{\Sigma}^{g'\to g}_{s,i,j,k} = \frac{\left\langle \Sigma^{g'\to g}_{s,i,j,k} \phi^{g'}_{i,j,k} \right\rangle}{\left\langle \phi^{g}_{i,j,k} \right\rangle}, \tag{2.52b}$$

$$\overline{\nu\Sigma}^{g'\to g}_{f,i,j,k} = \frac{\left\langle \nu\Sigma^{g'\to g}_{f,i,j,k} \phi^{g'}_{i,j,k} \right\rangle}{\left\langle \phi^{g}_{i,j,k} \right\rangle}, \tag{2.52c}$$

$$\overline{\phi}^{g}_{i,j,k} = \left\langle \phi^{g}_{i,j,k} \right\rangle. \tag{2.52d}$$

For anisotropic scattering, we would also have

$$\overline{\Sigma}^{g}_{tr,i,j,k} = \overline{\Sigma}^{g}_{t,i,j,k} - \sum_{g'=1}^{G} \overline{\Sigma}^{g'}_{s1,i,j,k}.$$

With diffusion approximation, Eq. (A.13) becomes

$$f^{(l+1),g}_{1,i\pm1/2,j,k} = \mp\frac{2}{3}\left(\frac{f^{(l+1),g}_{0,i\pm1,j,k} - f^{(l+1),g}_{0,i,j,k}}{\overline{\Sigma}^{g}_{t,i,j,k} h_{i\pm1} + \overline{\Sigma}^{g}_{t,i,j,k} h_i}\right), \tag{2.53}$$

and could accommodate boundary cells with albedo boundary condition [47]:

$$f^{(l+1),g}_{1,i\pm1/2,j,k} = \pm\frac{2(1-\beta^{g}_{i\pm1/2,j,k})}{4(1+\beta^{g}_{i\pm1/2,j,k}) + 3(1-\beta^{g}_{i\pm1/2,j,k})\overline{\Sigma}^{g}_{t,i,j,k} h_i} f^{g}_{0,i,j,k}. \tag{2.54}$$

Let $\tilde{D}^g_{i+1/2,j,k} = \frac{2}{3(\overline{\Sigma}^g_{t,i+1,j,k}h_{i+1}+\overline{\Sigma}^g_{t,i,j,k}h_i)}$, and the FDSA equation, Eq. (2.42), becomes

$$
\begin{aligned}
&-\frac{\tilde{D}^g_{i+1/2,j,k}}{h_i}f^g_{0,i+1,j,k}-\frac{\tilde{D}^g_{i,j+1/2,k}}{h_j}f^g_{0,i,j+1,k}-\frac{\tilde{D}^g_{i,j,k+1/2}}{h_k}f^g_{0,i,j,k+1}\\
&\quad+2\Big(\frac{\tilde{D}^g_{i+1/2,j,k}}{h_i}+\frac{\tilde{D}^g_{i+1/2,j,k}}{h_j}+\frac{\tilde{D}^g_{i+1/2,j,k}}{h_k}+\frac{\tilde{D}^g_{i+1/2,j,k}}{h_i}+\frac{\tilde{D}^g_{i+1/2,j,k}}{h_j}+\frac{\tilde{D}^g_{i+1/2,j,k}}{h_k}\Big)f^g_{0,i,j,k}\\
&\qquad-\frac{\tilde{D}^g_{i+1/2,j,k}}{h_i}f^g_{0,i-1,j,k}-\frac{\tilde{D}^g_{i,j+1/2,k}}{h_j}f^g_{0,i,j-1,k}-\frac{\tilde{D}^g_{i,j,k+1/2}}{h_k}f^g_{0,i,j,k-1}\\
&\qquad+\Big(\overline{\Sigma}^g_{t,i,j,k}-\sum_{g'=1}^{G}\overline{\Sigma}^{g'\to g}_{s,i,j,k}-\frac{\sum_{g'=1}^{G}\overline{\nu\Sigma}^{g'\to g}_{f,i,j,k}}{k^{(l+1/2)}}\Big)f^g_{0,i,j,k}\\
&\qquad=\frac{\sum_{g'=1}^{G}\overline{\nu\Sigma}^{g'\to g}_{f,i,j,k}\overline{\phi}^{(l+1/2),g}_{i,j,k}}{k^{(l+1/2)}}-\frac{\sum_{g'=1}^{G}\overline{\nu\Sigma}^{g'\to g}_{f,i,j,k}\overline{\phi}^{(l),g}_{i,j,k}}{k^{(l)}},
\end{aligned}
\tag{2.55}
$$

for an internal cell. The above system of equations could form a diagonal dominant matrix with the fission synthetic operator as the source term. This system of equations could then be solved to acquire the FDSA correction terms $f^g_{0,i,j,k}$ which are applied to the transport eigenfunction

$$
\overline{\phi}^{(l+1),g}_{i,j,k}=\overline{\phi}^{(l+1/2),g}_{i,j,k}+d\times f^g_{0,i,j,k}, \tag{2.56}
$$

where d is the damping factor used only in active cycles to avoid negative fluxes.The corrected eigenvalue could be evaluated with

$$
k^{(l+1)}=k^{(l+1/2)}\times\frac{\sum_{g'=1}^{G}\overline{\nu\Sigma}^{g'\to g}_{f,i,j,k}\overline{\phi}^{(l+1),g}_{i,j,k}}{\sum_{g'=1}^{G}\overline{\nu\Sigma}^{g'\to g}_{f,i,j,k}\overline{\phi}^{(l+1/2),g}_{i,j,k}}. \tag{2.57}
$$

This finite volume scheme is applied to our OpenMC-FDSA implementation for 2D full core calculations.

2.3 Implementation of multigroup FDSA

The discretized FDSA method has been implemented into a S_N and a hybrid MC solver, the approach of which will be introduced in this section. The implementation processes for the two types of solvers are similar in general, with the normalizations of flux and applying corrections at each power iteration in transport calculation. This is one of the features specifically designed to achieve the adaptability across different solvers.

2.3.1 Implementation in multigroup S_N solver

For demonstration purposes, a 1D multigroup S_N solver is developed with Diamond Differencing and Gauss-Legendre angular quadrature sets up to S_{32} taken from the book [48]. Along with the FDSA method, other comparable methods such as DSA and CMFD are also implemented in this S_N solver. A mesh-refinement study was carried out to validate the implementation process and the results are included in Appendix-B.2.

A two-level approach, similar to research done on multilevel methods [3, 7], is taken. However, the possibilities of applying FDSA in multilevel methods do not stop here. The two inputs including flux and eigenvalue, do not need to come from the same transport calculation. This feature has not been investigated adequately at this moment and thus will be excluded from the planned work.

The implementation of FDSA in the S_N solver is completed according to the following algorithm:

Algorithm 1: Iterative scheme for the FDSA method.

Power iteration l:

while $|k^{(l+1)} - k^{(l)}| > (1/\rho_k - 1)\,\varepsilon_k$ *or* $\|\phi^{(l+1)} - \phi^{(l)}\|_\infty > \left(1/\rho_\phi - 1\right)\varepsilon_\phi^{PI}$ **do**

Level 1: Transport calculation:

for g=*1, ... ,G* **do**

Calculate up-scattering source $\frac{1}{2}\sum_{g'=g+1}^{G}\Sigma_{s,g'\to g,j}\phi_{g',j}^{(l-1)}$ and fission source $\frac{\chi_g}{2k^{(l)}}\sum_{g'=1}^{G}\nu_{f,g',j}\Sigma_{f,g',j}\phi_{g',j}^{(l-1)}$

end

for g=*1, ... ,G* **do**

Calculate down-scattering source $\frac{1}{2}\sum_{g'=1}^{g-1}\Sigma_{s,g'\to g,j}\phi_{g',j}^{(l)}$

Solve the transport equation, Eq. (2.29) for group g and obtain $\phi_{g,j}^{(l)}$

end

Calculate $k^{(l)}$

Normalize $\phi_{g,j}^{(l)}$ such that $\sum_j \phi_{g,j}^{(l)} = 1$

Level 2: Low-order FDSA calculation:

Solve FDSA equation Eq. (B.1) to obtain $\phi_{g,j}^{(l+1)}$

Normalize $\phi_{g,j}^{(l+1)}$ such that $\sum_j \phi_{g,j}^{(l+1)} = 1$

Calculate $k^{(l+1)}$ with Eq. (2.24)

Calculate $\rho_k = \frac{\|\phi^{(l+1)}-\phi^{(l)}\|_\infty}{\|\phi^{(l)}-\phi^{(l-1)}\|_\infty}$ and $\rho_\phi = \frac{|k^{(l+1)}-k^{(l)}|}{|k^{(l)}-k^{(l-1)}|}$

end

At the inner iteration level a DSA module has been implemented. It has been discovered that FDSA could be used with DSA since the two methods are applied at different level of acceleration. And with the CMFD module in comparison, the entire S_N solver functions according to the following flowchart:

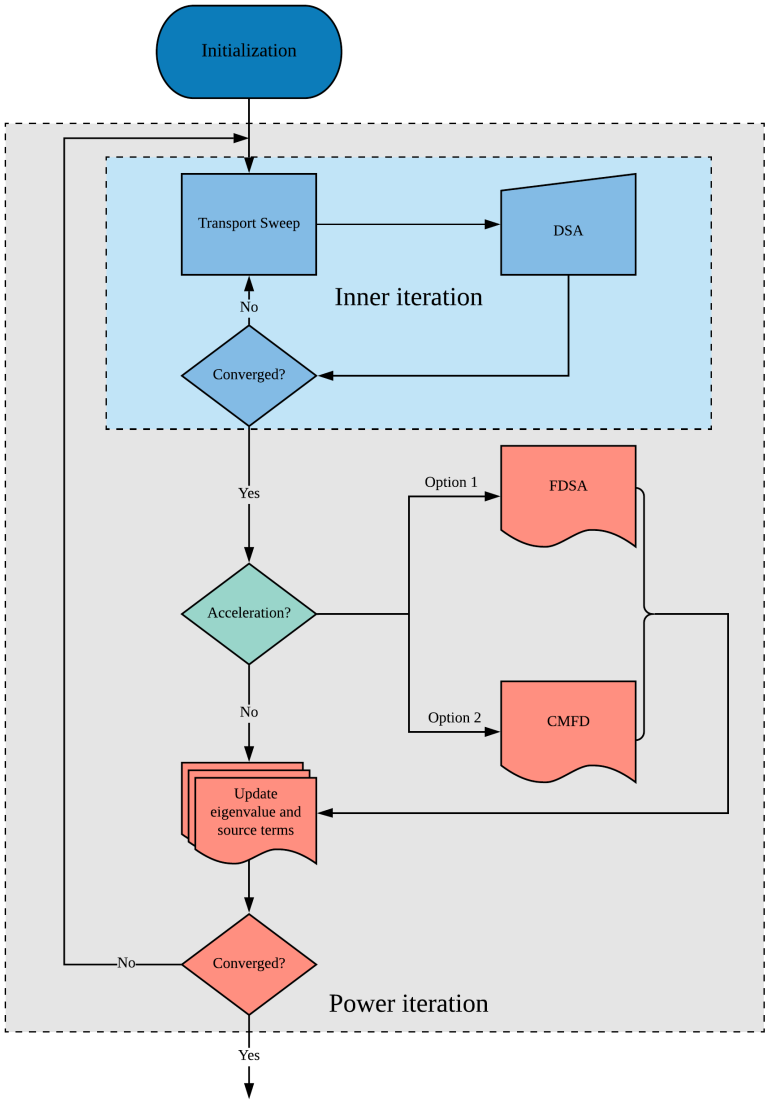

Figure 2.2: Iterative scheme of S_N solver.

2.3.2 Implementation in multigroup hybrid Monte Carlo solver

In terms of coding algorithm, the MC solver is somewhat similar to the deterministic one. Considering a standard transport calculation, a MC cycle is equivalent to the inner iteration where a fixed source problem is solved. As shown in the work on MC-DSA method [42], the

DSA method is not ideal for the application in a hybrid solver, thus no technique is applied within a MC cycle. This idea leads to the implementation approach in our work:

Algorithm 2: Hybrid scheme for MC-FDSA method.

MC Cycle l:

while $l <$ # *of inactive cycles* **do**

- Level 1: Transport calculation:
  1. Simulate a batch of neutrons to obtain $\phi_g^{(l+1/2)}$ and corresponding eigenvalue $k^{(l+1/2)}$;
  2. Normalize the flux tally according to total neutron weights.
- Level 2: Low-order FDSA calculation:
  1. Solve Eq. (B.1) and use Eq. (2.23) to acquire corrected flux $\phi^{(l+1)}$;
  2. Normalize the corrected flux $\phi_g^{(l+1)}$ such that $\sum_i \sum_g \phi_{i,g}^{(l+1)} = A$;
  3. Evaluate new eigenvalue $k^{(l+1)}$ with Eq. (2.24) or Eq. (2.25).
- Update fission neutron weights according to the corrected flux $\phi_g^{(l+1)}$.

Continue to next MC cycle.

end

In the event that the cross section data for MC solver is multigroup, the group constant generation step would not be necessary. However, since most applications of MC method are done with continuous energy cross sections, it is important that the development of hybrid neutronics methods includes this step and thus enables the application of these methods in continuous energy domain. The above algorithm could then be illustrated with Fig. 2.3.

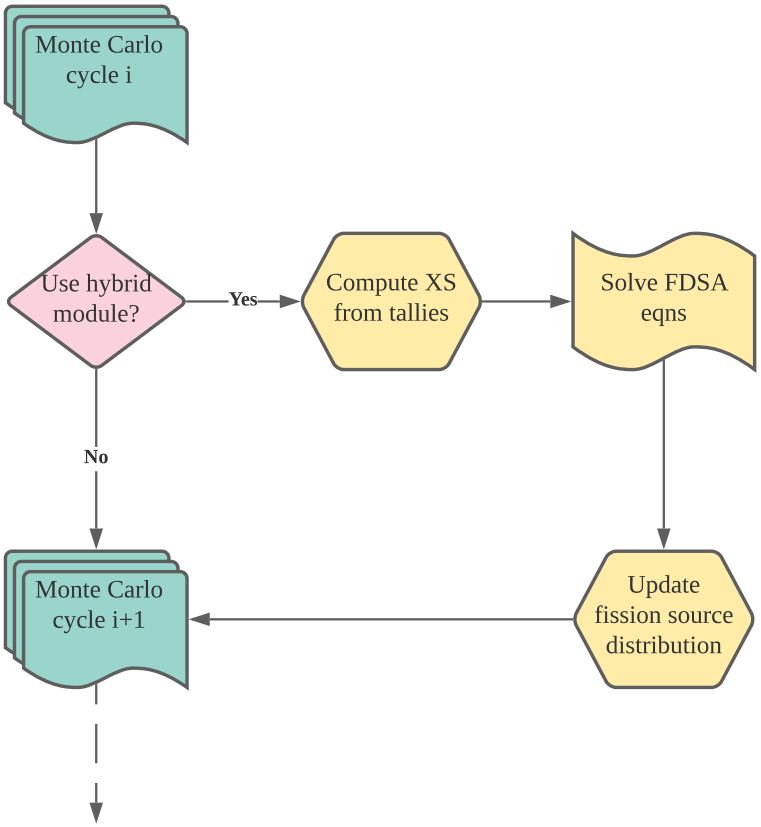

Figure 2.3: Algorithmic flowchart of MC-FDSA method.

The entire algorithm then focuses on a 3-step process within the hybrid module. Firstly the cross sections are computed with MC tallies that are predefined to capture all necessary information as introduced in Chapter 2. Then the low-order FDSA problem is constructed and solved with the cross sections, either in a matrix form for a problem smaller in dimension in space or energy, or in an iterative form similar to that of a diffusion equation. Lastly, the fission source distribution in the MC fission bank is updated with the corrected distribution through a weight-updating scheme.

To apply the corrected flux from FDSA to the neutron bank in OpenMC, the fission source needs to be calculated and the fission neutrons' weights updated correspondingly. There are

two approaches to accomplish this. One is described in detail in Herman's thesis [36] which computes the weights of each neutron directly based on its location in phase space. The other one, as introduced below, is to calculate the fission sources' ratio for each one location in phase space and to multiply the ratio to the neutron weights.

First we calculate the fission sources' ratio in phase space $(\vec{r}_j, E_g)$:

$$F_j = \frac{\sum_{g'=1}^{G} \nu_{f,g',j} \Sigma_{f,g',j} \phi_{g',j}^{(l+1)}}{\sum_{g'=1}^{G} \nu_{f,g',j} \Sigma_{f,g',j} \phi_{g',j}^{(l+1/2)}} \ . \tag{2.58}$$

For certain fission neutron born in phase space $(\vec{r}, E_g)$ with an original weight $w_{i,g}$, the updated neutron weight would be

$$w'_{g,j} = w_{g,j} \times F_j \ . \tag{2.59}$$

To ensure that the total neutron weight N stays the same, a normalization on the neutron weights is needed:

$$w''_{g,j} = w'_{g,j} \times \frac{N}{\sum_g \sum_j w'_{g,j}} \ . \tag{2.60}$$

Note that the fission spectrum is not included in the above equations. If the number of fission neutrons is large enough such that the count of fission neutrons in each group reflect the fission spectrum correctly, the fission spectrum is not needed in this process. This avoids counting the fission neutrons in each group and only adjusts their weights according to their locations in the model and thus can be executed faster. If the fission spectrum is extremely small in certain groups, or the number of neutrons used in MC calculation is not sufficiently large, this approach would lead to a different set of neutron weights. However, in such events, the statistical error in MC calculation would be too large to generate any meaningful results anyway. In brief, the two approaches of updating neutron weights are quite similar and would achieve the same results.

2.4 Summary

The derivation and discretization of the FDSA method is introduced and explained in detail in this chapter, together with the implementation approach of such a method in both S_N and hybrid solver. The theoretical advantages and possible obstacles the FDSA method might bring are also discussed in terms of the complexity of low-order problem, computational costs in solving said problem, and implementation algorithm. In general the FDSA method is similar to DSA in the sense that two transport inputs are required and the low-order problem is only solved once. Since the low-order problem is not an eigenvalue problem itself, its convergence and stability behavior is expected to be different from the more popular acceleration methods such as CMFD and QD. These behaviors are explored and investigated in Chapter 3 with numerical results in different space and energy models.

CHAPTER

3

NUMERICAL RESULTS: SOURCE CONVERGENCE ACCELERATION

The path for the development of FDSA is of course not certain from the very beginning, and a top-down approach was taken to first demonstrate the feasibility of such a method both theoretically and numerically. Also, the acceleration of source convergence was the first and only goal at the beginning of this project with the variance reduction features added later. Thus we separate the numerical investigations of these two subjects into two chapters and include the results on source convergence acceleration in this one.

The first FDSA module was created with one-group derivation included in Appendix-A.1 in

the form of consistent discretization described in detail in Urbatsch's thesis [16]. Though the two methods are quite different, the discretization approach is essentially the same, thus omitted here. However, the impact brought by inconsistent discretization, a topic which was crucially important for traditional DSA method, is not investigated for the FDSA method introduced in this thesis because a) Urbatsch's work found no noticeable difference between the two ways of discretizations for various physical problems or in deterministic and hybrid methods, and b) for the multigroup FDSA in Chapter 2, a cell-edge consistent discretization is rather burdensome both mathematically and numerically. However, this might be added to the future work should the viewers find it necessary.

Several cases in slab geometry were created with artificial one-group cross sections and the results satisfyingly demonstrated that the FDSA method functions as intended, though not as well as CMFD. With its feasibility proven, the method was extended to multigroup calculations, with discretizations and implementations introduced in Chapter 2. The implemented multigroup FDSA method was then tested with both homogeneous and heterogeneous cases.

After the feasibility of such a hybrid neutronics method is proved with the multigroup cases, the extension to continuous energy simulation was implemented and tested first with a 1-D homogeneous slab case with artificial material composition and later several 2-D heterogeneous cases including the C5G7 [49] full core calculation.

3.1 One-group calculations in slab geometry

The one-group calculations were completed with both the deterministic and hybrid solvers and are discussed here.

3.1.1 One-group deterministic results

A heterogeneous case in slab geometry with alternating fuel and absorber is used to test the deterministic solver with FDSA module. This heterogeneous slab has the following configurations:

1. Cross section of Fuel: $\Sigma_t = 1.0, \Sigma_s = 0.7, \nu\Sigma_f = 0.3071$
2. Cross section of Absorber: $\Sigma_t = 1.0, \Sigma_s = 0.001, \nu\Sigma_f = 0.0$
3. Uniform lattice, 29 *cm* thick slab with alternating $2cm$ fuel regions and 1 *cm* absorber regions
4. Using reflective BC on the left side and vacuum BC on the right side

The geometry of this case is shown in Fig. 3.1, with fuel shown in red and absorber in blue.

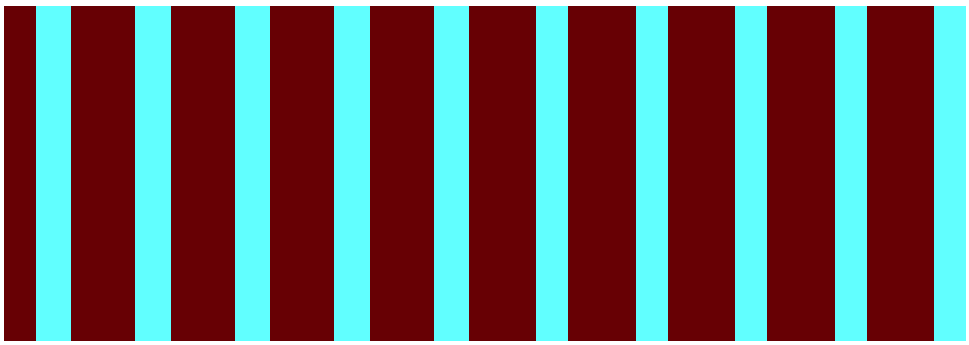

Figure 3.1: Geometry of the heterogeneous slab.

A uniform mesh with $h = 0.126$ *cm*, or 16 meshes for each centimeter in fuel or absorber region, is used in the S_{32} solver. The convergence criteria on the flux and eigenvalue is $\varepsilon_\phi^{PI} = 10^{-8}, \varepsilon_k = 10^{-7}, \varepsilon_\phi^{IN} = 10^{-8}$. Because of the highly absorbing regions, the dominance ratio of this case is 0.996 [16], which leads to a very large number of PI in transport calculations.

The eigenvalues and numbers of transport sweeps in both high and low-order calculations are included in Table 3.1. The power iterations in CMFD are completed without wielandt's shift method.

Table 3.1: Eigenvalues in transport sweeps and iterations with heterogeneous slab case.

Mode	Eigenvalue	No. of transport sweeps	No. of iterations in low-order problem
S_N	0.59852533	2334	0
S_N+FDSA	0.59852533	136	136
S_N+CMFD	0.59852501	11	1304

The comparison among the standard transport solver, the FDSA method and the CMFD method is discussed here. Not surprisingly, the CMFD method converges with a slight difference in eigenvalue since an inconsistent discretization [7], is used in the implementation process. This can easily be minimized by tight convergence criteria in the low-order calculation. Since the one-group FDSA method is implemented with cell-edge consistent discretization, the eigenvalue it achieves is identical to that of the transport calculation. However, in terms of reducing the number of transport sweeps, the CMFD method is more superior by a large factor in this case, 10 times less than the FDSA method at the cost of 10 times more iterations in low-order problem.

Since the low-order diffusion-like problems are, in general, much easier to solve than the transport problem, it's ideal to have a lower number of iterations in transport problem. On the other hand, an increasing number of iterations in low-order problem might neutralize the efficiency improvement brought by such acceleration methods. The heterogeneous case here is rather extreme with the high dominance ratio and in realistic cases the gap between CMFD and FDSA might not be so distinct.

3.1.2 One-group hybrid MC-FDSA results

After demonstrating that the FDSA method functions as intended in the S_N solver, the same heterogeneous slab case, as shown in Fig. 3.1, is then solved with the hybrid MC-FDSA solver and the results are compared against the standalone MC calculation with OpenMC, which has an externally coupled FDSA module. However, without a direct way of monitoring the source convergence process, only the flux distribution at certain cycles are compared. The standalone OpenMC calculation would require around 300 MC cycles with 1 million particles per cycle to reach source convergence, while with FDSA feedback, this could be reduced to 20-30 cycles, as illustrated in Fig. 3.2.

Figure 3.2: Flux comparison for hybrid solver and OpenMC.

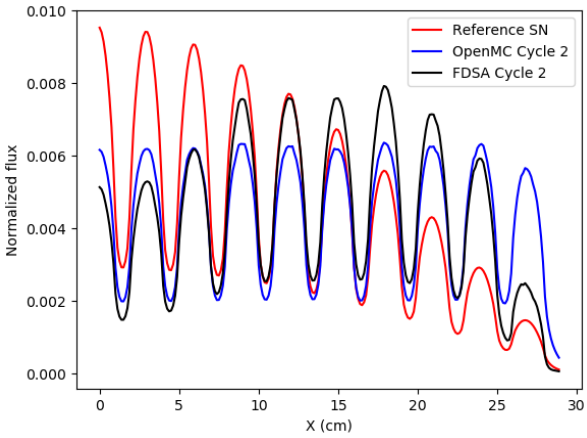

(a) Cycle 2.

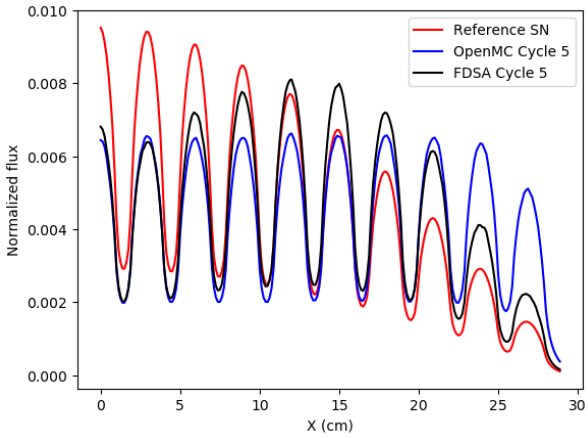

(b) Cycle 5.

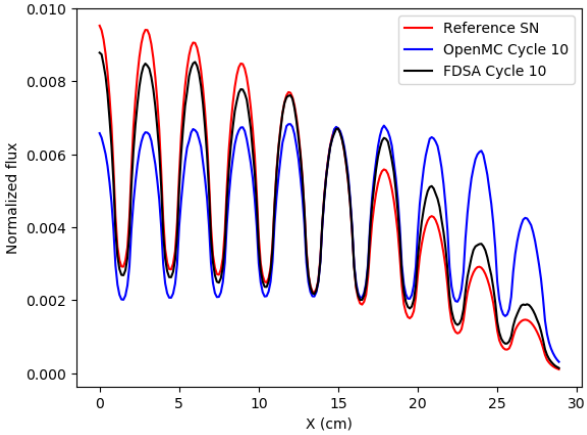

(c) Cycle 10.

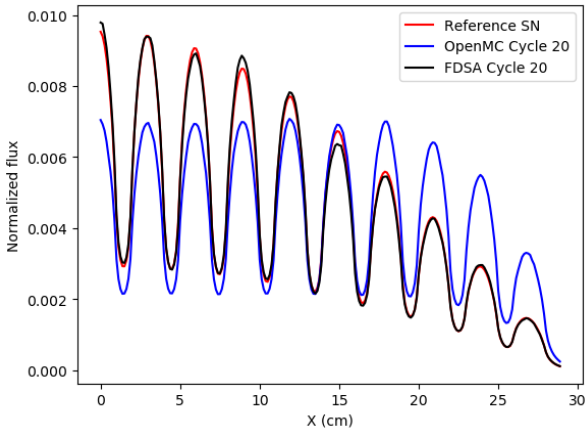

(d) Cycle 20.

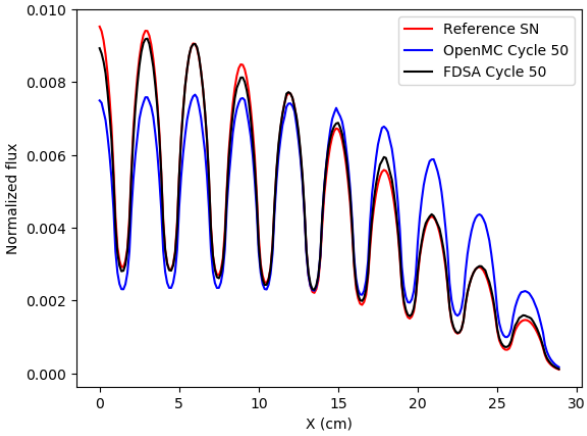

(e) Cycle 50.

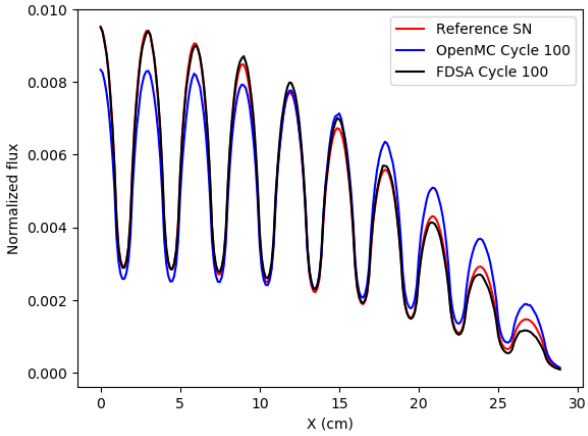

(f) Cycle 100.

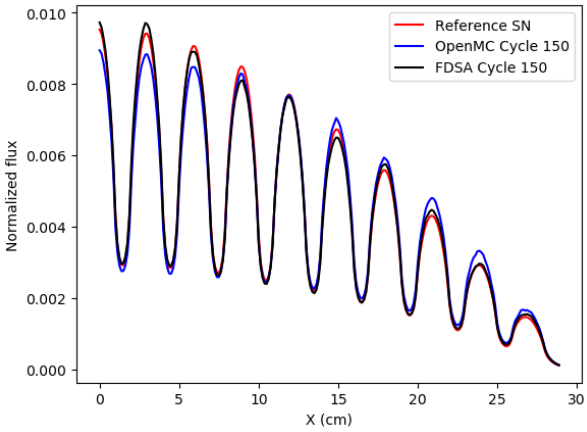

(g) Cycle 150.

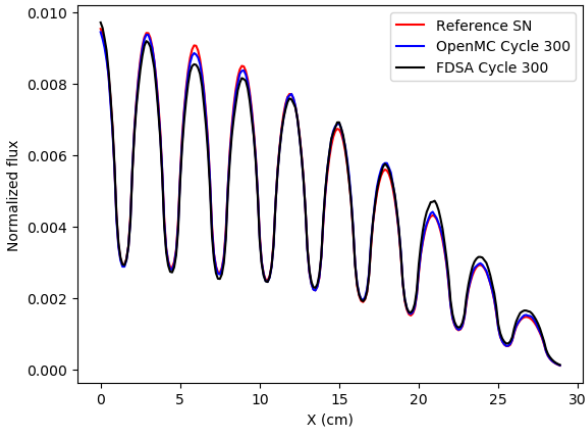

(h) Cycle 300.

The flux and error in flux comparison is illustrated in Fig. 3.3, at the points where convergence is achieved for standalone OpenMC and the hybrid solver. At Cycle 20, the magnitude of error with MC-FDSA is reduced to about 10^{-4}, which is close to the final results from the reference case. The standalone OpenMC would require about 300 cycles to achieve this, as shown in Fig. 3.3b.

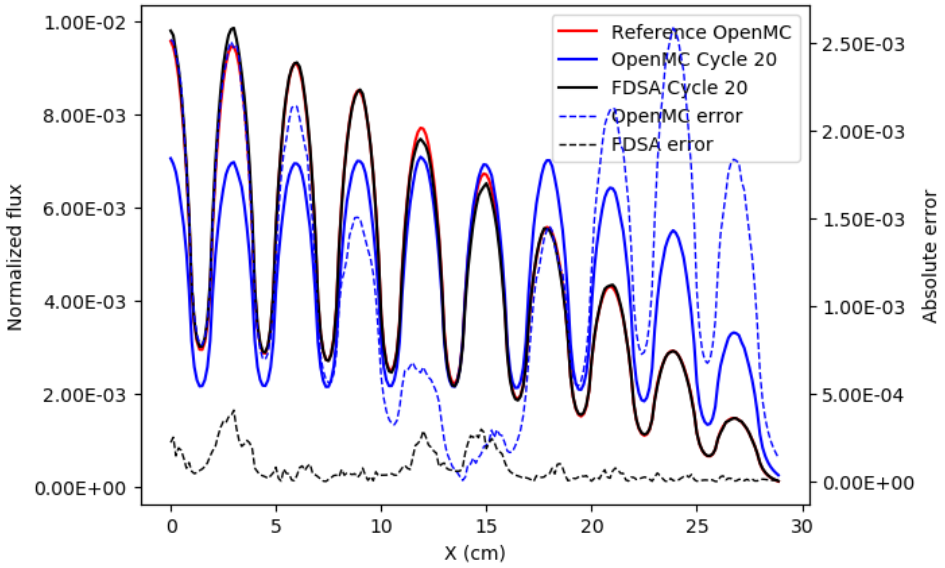

(a) Cycle 20.

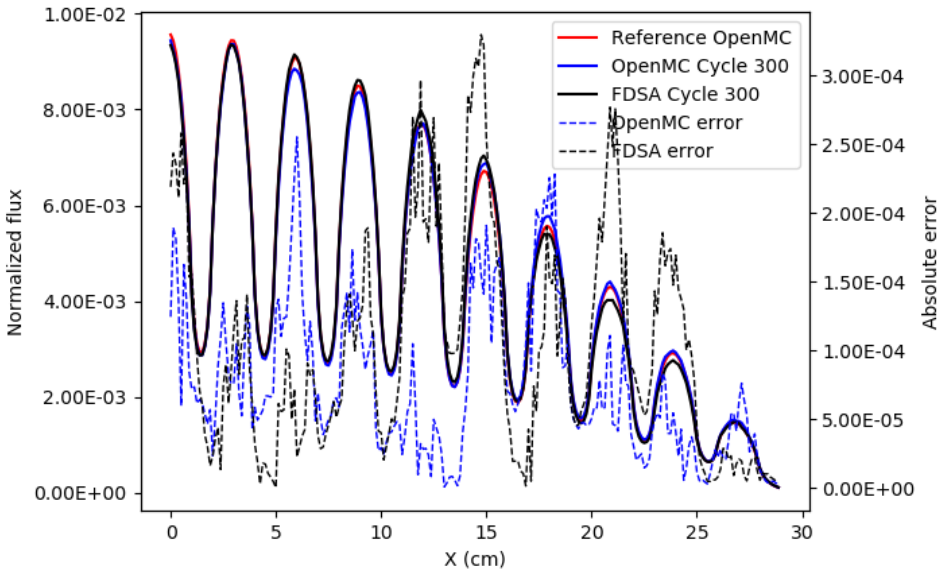

(b) Cycle 300.

Figure 3.3: Flux and error comparison in one-group test for hybrid solver and OpenMC.

This convergence behavior in the hybrid solver is similar to that in the deterministic solver. The comparison of Shannon entropy [19] of the two cases, shown in Fig. 3.4, agrees with this convergence behavior, where the MC calculation slowly converges the fission source and the

FDSA feedback would force this convergence at the very beginning. What's more intriguing is that the FDSA feedback introduces a larger oscillation in the Shannon entropy. This does not translate into a large uncertainty in the actual flux, as shown in Fig. 3.2, but rather indicates that the FDSA feedback has a strong "correcting" effect on the MC flux convergence.

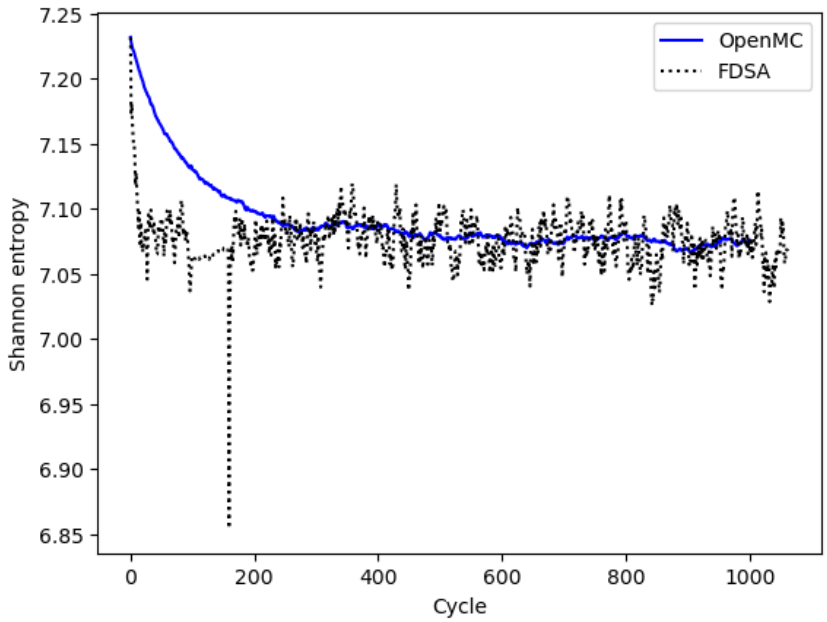

Figure 3.4: Shannon entropy of OpenMC and hybrid solver in one-group test.

The runtime used by OpenMC and the hybrid solver is included in Table 3.2. Even though the FDSA module is externally coupled, the impact on the MC solver is minimal in terms of the actual runtime compared to the intensive transport calculation.

Table 3.2: Number of inactive cycles and runtime comparison of OpenMC and hybrid solver.

Solver	No. of inactive cycles	Runtime (s)
OpenMC	300	461.4
OpenMC+FDSA	20	46.3 (0.6 in FDSA)

Much effort were committed to this stage of development as it was the first time that the FDSA scheme was proved to be at least functioning. Even though the comparison is somewhat fragmented without a hybrid MC-CMFD solver for the multigroup simulations, we acquired the first sets of results that give us the ground on which the MC-FDSA method could be evaluated. With the possibility to accelerate the power iterations for eigenvalue problems with normalization, we moved on to multigroup calculations for more realistic problems.

3.2 Multigroup calculations in slab geometry

The implementation of multigroup FDSA was firstly tested with an infinite homogeneous problem with 2-group artificial cross sections and then proceeded to heterogeneous cases with 7-group cross sections. In the matrix form, the system of equations for 2-group FDSA would take the form of:

$$LHS = \begin{pmatrix} \begin{bmatrix} a_{11} & a_{12} & \\ a_{21} & \ddots & \ddots \\ & \ddots & \ddots \end{bmatrix} & \begin{bmatrix} b_{11} & & \\ & \ddots & \\ & & \ddots \end{bmatrix} \\ \begin{bmatrix} c_{11} & & \\ & \ddots & \\ & & \ddots \end{bmatrix} & \begin{bmatrix} d_{11} & d_{12} & \\ d_{21} & \ddots & \ddots \\ & \ddots & \ddots \end{bmatrix} \end{pmatrix}$$

All sub-matrices are sparse matrices. The a_{nn} and d_{nn} matrices are the matrices for the current groups while the b_{nn} and c_{nn} are the group to group coupling. This matrix is made up of four diagonal dominant matrix and in a whole, diagonal dominant itself. For physical problems in 1D, up to 7 energy groups, the matrix is not that big and is efficiently solved with a linear algebra package. When more energy groups are added, which is not ideal for acceleration purpose, or when we move to multi-dimensional problems, this matrix will expand significantly, hence an successive over relaxation (SOR) solver will be needed at a later stage.

3.2.1 Multigroup deterministic results

To conduct a comprehensive test with features like multigroup cross section, heterogeneous material configuration and one-dimensional geometry, the following test was modified and

designed from the C5G7-TD benchmark [49] and work on NDA [7]. It consists of two fuel assemblies shown in Fig. 3.5, each with 17 pins and 21.42 cm in width.

Reflection	MOX	UO2	Reflection
	$\leftarrow 21.42\ cm \rightarrow$	$\leftarrow 21.42\ cm \rightarrow$	

Figure 3.5: Geometry of the 2-group 4-pin test.

The pin configuration in each assembly is shown in Figs. 3.6 and 3.7. The assemblies are made of alternating fuel and guide tube materials.

UO_2	UO_2	GT	UO_2	UO_2	GT	UO_2	UO_2	GT	UO_2	UO_2	GT	UO_2	UO_2	GT	UO_2	UO_2

Figure 3.6: Geometry of UO2 assembly.

MOX43	MOX70	GT	MOX87	MOX87	GT	MOX87	MOX87	GT	MOX87	MOX87	GT	MOX87	MOX87	GT	MOX70	MOX43

Figure 3.7: Geometry of MOX assembly.

For UO_2 and MOX pins, the pin geometry is heterogeneous as shown in Fig. 3.8. Each pin is 1.26 cm in width and divided into 14 meshes, 12 in fuel and 2 in moderator.

Moderator	Fuel	Moderator
0.09 cm	$\leftarrow$1.08 cm$\rightarrow$	0.09 cm
1 mesh	12 meshes	1 mesh

Figure 3.8: Geometry of fuel pin.

And the guide tube is homogeneous with only one material.

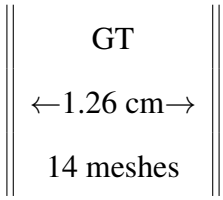

Figure 3.9: Geometry of guide tube.

With this 7-group heterogeneous case the FDSA method's performance could be examined. The convergence criteria is $\varepsilon_{\phi}^{PI} = 10^{-8}, \varepsilon_{k} = 10^{-7}, \varepsilon_{\phi}^{IN} = 10^{-8}$. The results are then compared against transport and CMFD calculations. The eigenvalues and number of power iterations consumed of these calculations are included in Table 3.3.

Table 3.3: Eigenvalues and number of power iterations in 2-assembly test.

Solver	S_N	S_N+FDSA	S_N+CMFD
No. of transport sweep in each group	40	16	11
No. of PI in low-order problem	0	16	653
k_{inf}	1.10953426	1.10953454	1.10954625

With only reflective boundary condition, the FDSA calculation updates the fission source much less frequently and thus the acceleration effect brought by FDSA is less compared to the above tests. Nevertheless a 40-50% acceleration in terms of number of iterations could be achieved with FDSA. The comparison against CMFD is somewhat similar to that in the one-group problem, in that though it needs less iterations in transport calculations, the CMFD method would add on a much larger number of power iterations in the low-order problem.

Whether this indicates the superiority in either method depends on the physical problem and how the solvers, both transport and diffusion ones, are constructed and optimized. However, for cases with more moderation such as this one, the FDSA method seems to perform better than itself in the one-group case with more absorption. Further, the FDSA method arrives at the transport eigenvalue while the CMFD method does not. This comes as a surprise since the discretization of multigroup FDSA Eqs. (2.42) and (2.43) is inconsistent with the transport equation Eq. (2.26).

With the success of multigroup FDSA in the S_N solver, we proceeded to its investigation in the hybrid solver.

3.2.2 Multigroup MC-FDSA results

The above 2-assembly heterogeneous case is then constructed for the hybrid MC-FDSA solver and the same case is run with OpenMC in comparison. These two cases are completed with 1 million particles per cycles and the reference OpenMC calculation is done with the same number of particles and 1,000 cycles (100 inactive). Though we focus on validating the effectiveness of FDSA, a quick check is done on the eigenvalue so that the MC calculations provide similar outcomes. The eigenvalues from the S_N solver, the hybrid solver and OpenMC are included in Table 3.4.

Table 3.4: Eigenvalue comparison of 1D 7-group 2-assembly test with S_N and hybrid solvers.

Solver	Eigenvalue
S_N	1.10953426
Hybrid	1.11023637
OpenMC	1.11020±0.00002

Though the difference in eigenvalue between OpenMC and the S_N solver is large which could be attributed to the discretization error and approximations like Diamond Difference, the MC-FDSA solver converges quite well at the 100th cycle to OpenMC. Since the hybrid solver produces results in good agreements with OpenMC, we proceeded to examine the flux convergence process which is more important in the development of the hybrid method.

The flux convergence is checked at certain cycles between MC-FDSA and OpenMC. To ensure that the FDSA module is providing correct feedback towards OpenMC, the flux distribution after the first FDSA calculation, from Group 1 through Group 7, is checked, as shown in Fig. 3.10.

Figure 3.10: Spatial flux distribution in Cycle 2 of 1D 7-group 2-assembly test.

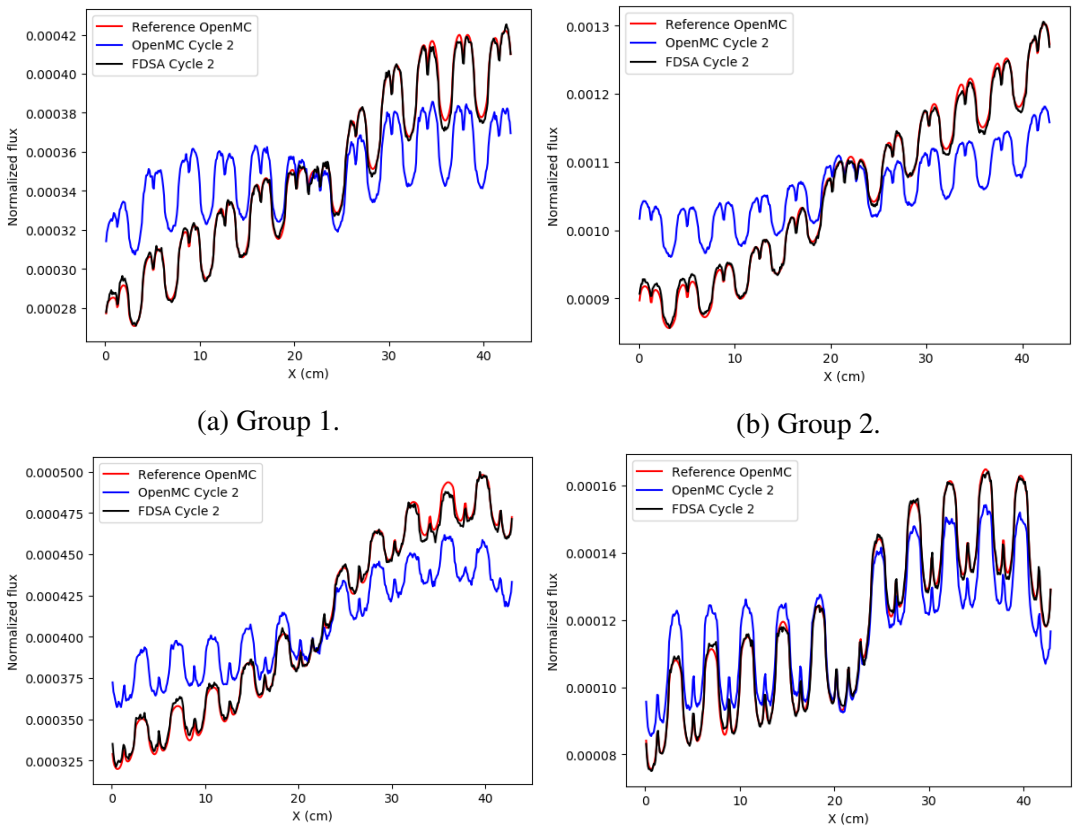

(a) Group 1.

(b) Group 2.

(c) Group 3.

(d) Group 4.

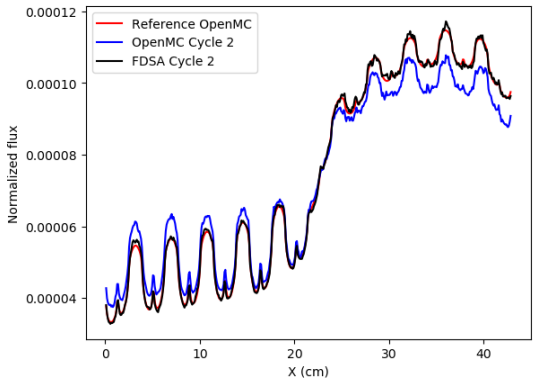

(e) Group 5.

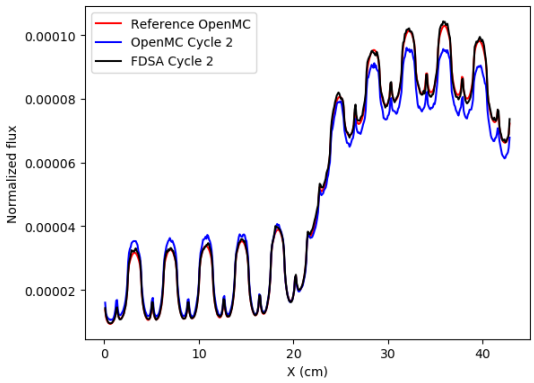

(f) Group 6.

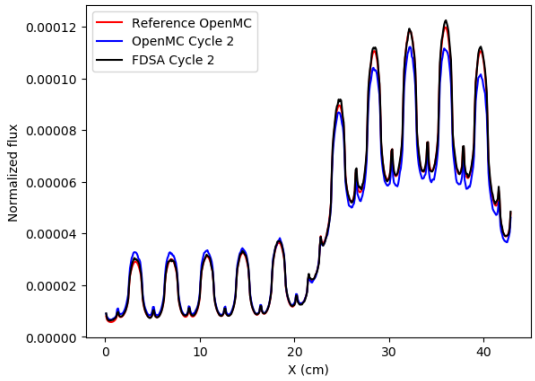

(g) Group 7.

Overall FDSA provides correct feedback in the hybrid solver and with it the flux distribution converges immediately, even only applied once. Across the 7 groups, the first few groups seem to be more difficult to converge which is expected since the flux magnitude is larger in those groups. Due to the difficulty in converging fluxes in higher energy groups, the flux in the first group is then examined in different cycles to monitor the flux convergence process, included in Fig. 3.11.

Figure 3.11: Spatial flux distribution of group 1 in different cycles.

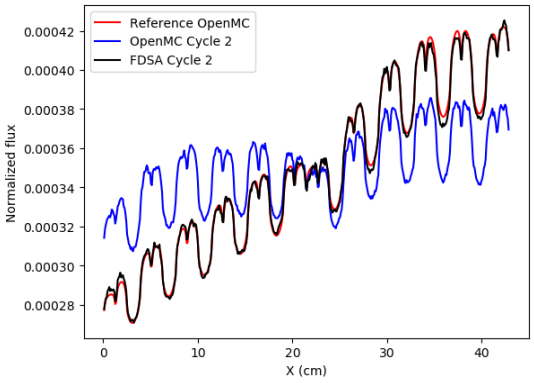

(a) Cycle 2.

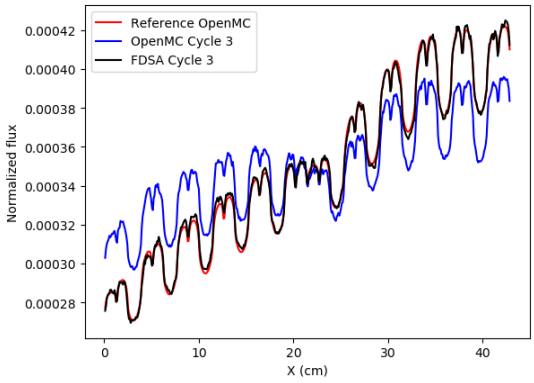

(b) Cycle 3.

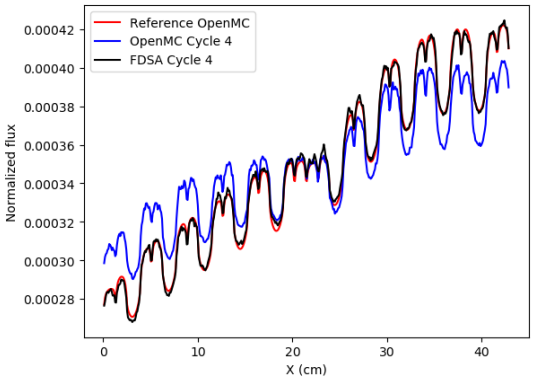

(c) Cycle 4.

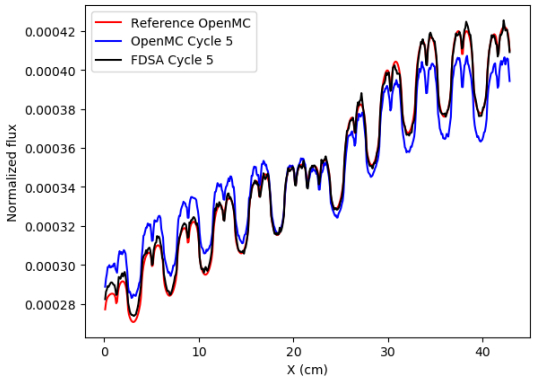

(d) Cycle 5.

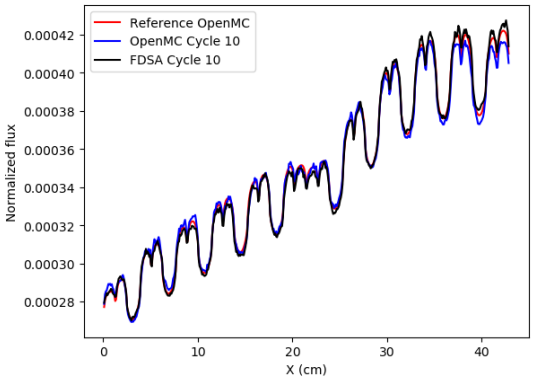

(e) Cycle 10.

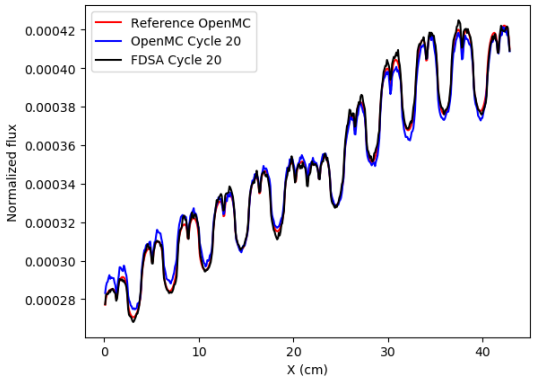

(f) Cycle 20.

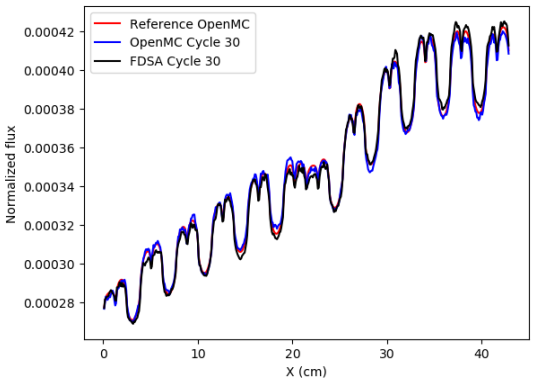

(g) Cycle 30.

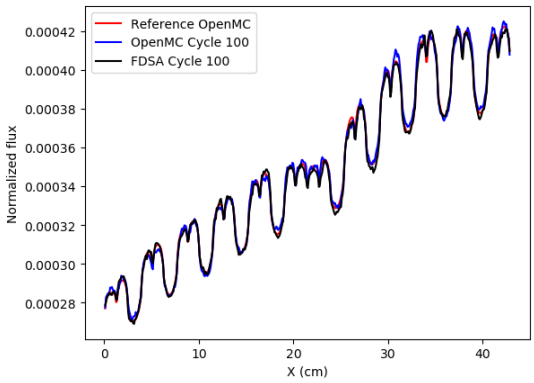

(h) Cycle 100.

For a close look, the flux distributions and the absolute error in flux at Cycle 2 and Cycle 10 are included in Fig. 3.12.

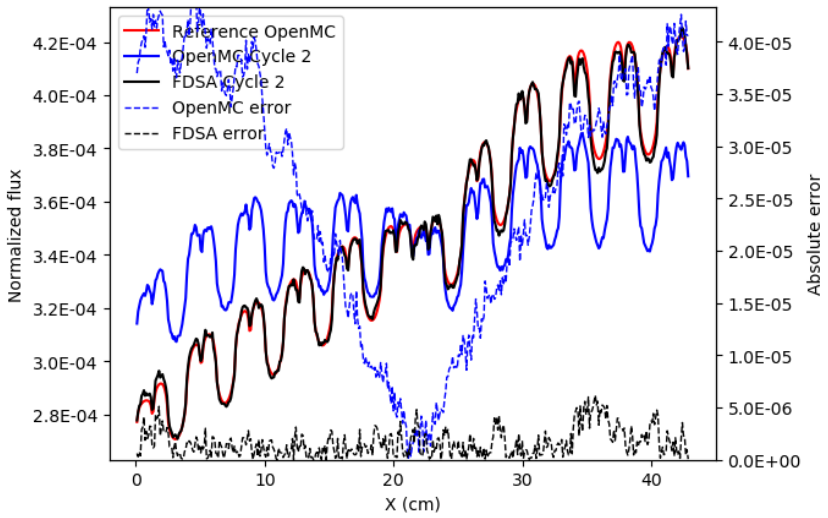

(a) Flux in Group 1, Cycle 2.

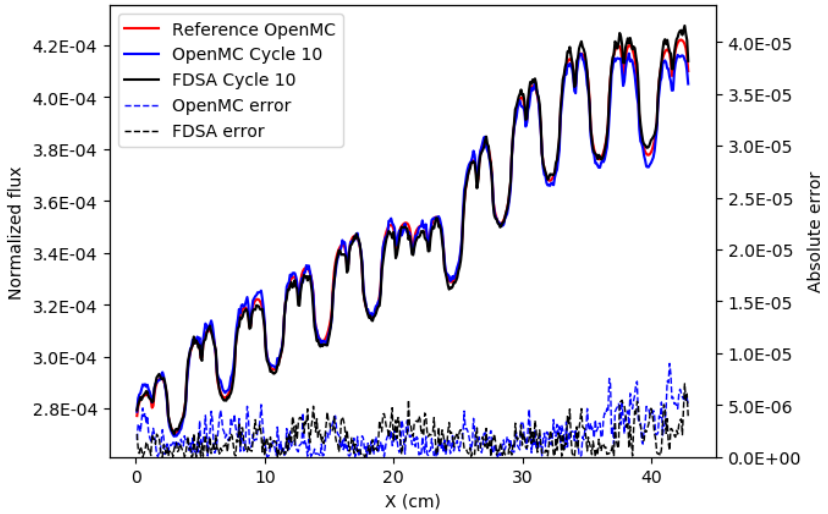

(b) Flux in Group 1, Cycle 10.

Figure 3.12: Flux and absolute error in multigroup test for hybrid solver and OpenMC.

Judging from the flux distribution, the standalone OpenMC could converge the fission source at around 10-20 cycles. Similar to the one-group case, the source convergence in MC calculation could be accelerated by a factor of about 10. However, since the number of cycles needed by the original MC calculation is so small, it's probable that the actual speedup is better. To confirm this acceleration effect, Shannon entropy of these two cases is compared over the 100 inactive

cycles, in Fig. 3.13.

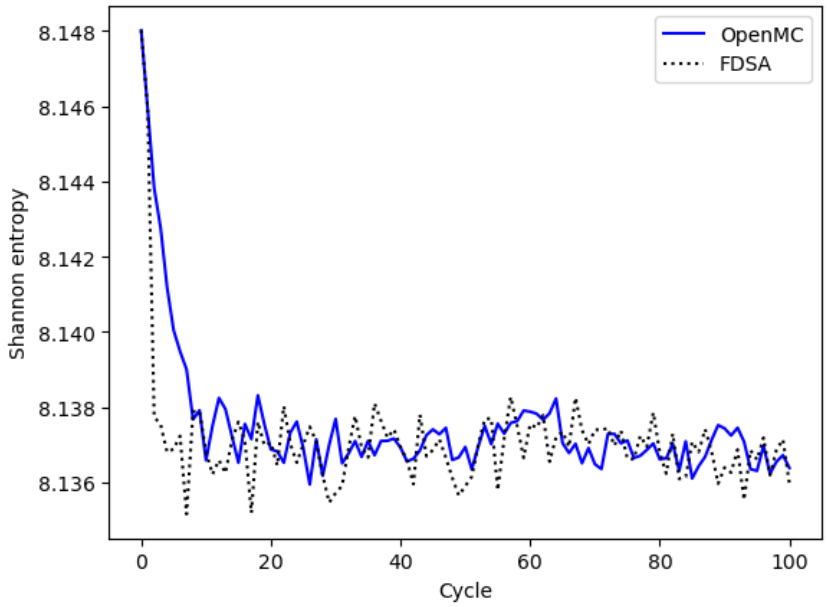

Figure 3.13: Shannon entropy in 1D 7-group 2-assembly test.

The immediate drop of Shannon entropy of corrected flux indicates that the FDSA feedback provides the acceleration needed and as shown in the Fig. 3.11, standalone OpenMC catches up at around 10-20 cycles. The general trend of flux convergence process is the same as the one-group case, though less extreme. This concludes the numerical experiments of FDSA in both deterministic and stochastic applications.

3.3 Continuous energy MC-FDSA results

To meet the demand of a continuous energy solver with which most MC applications are completed, the extension to continuous energy was finished. A sequence of tests were completed firstly to conduct validation and verification on the solver, and secondly to assess the MC-FDSA

performance in this new simulation mode. Two of these tests, a homogeneous slab test and a C5G7 full core case, are selected to be presented here. With the MC-CMFD module in OpenMC, we are able to conduct a side by side comparison with the two methods.

3.3.1 Continuous energy homogeneous slab case

The first test features a 70 cm wide homogeneous slab with artificial material composition [36] shown in Table 3.5. The boundary conditions on both ends of the slab are vacuum, the treatment of which is done with albedo boundary condition introduced in Chapter 2 for the low order problems. The spatial mesh for both Shannon entropy calculation and low order problems is a uniform 1 cm wide mesh and the 1-group cross sections are computed with MC tallies at the end of each MC cycle. In order to ensure a relatively high quality in tallying results, 2 million particles per cycle is used with 50 inactive and 150 active cycles in MC simulation. The reference case is, on the other hand, completed with 5 million particles per cycle and 500 cycles (50 inactive) in total.

Table 3.5: Homogeneous slab material composition.

Density	19.0 gram/cm^3
U_{235} weight percent	0.21
U_{238} weight percent	0.68
O weight percent	0.11

Thanks to the readily available MC-CMFD solver in OpenMC, this first test contributes to the comparison of MC-FDSA and MC-CMFD in the continuous energy simulations. To manifest the effectiveness of the hybrid solvers, a standalone MC simulation with OpenMC is

also included in the comparison. First we examine the Shannon entropy of the 3 cases with a baseline from the reference case, plotted in Fig. 3.14. Since MC-CMFD could be applied at the end of first cycle, its effect on source convergence is seen in Cycle 2, while the MC-FDSA would require 2 cycles' inputs thus its effect starts in Cycle 3. Nevertheless, both methods behave as intended in accelerating the source convergence process and the convergence is achieved again almost instantly like it is in the multigroup case with the feedback from MC-FDSA. While the standalone MC simulation needs about 15 cycles to converge, the MC-CMFD converges at Cycle 2 and MC-FDSA converges at Cycle 3, both of which is when the feedback is first applied.

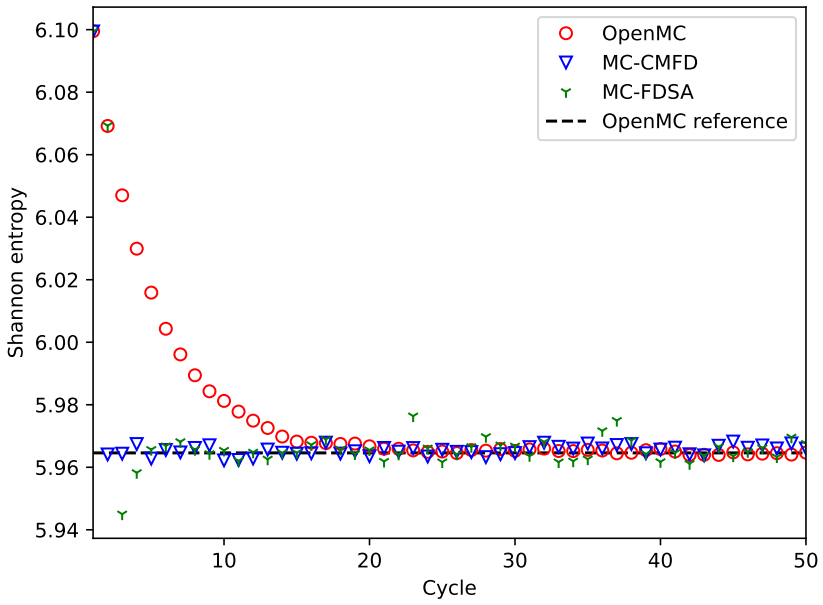

Figure 3.14: Shannon entropy of the homogeneous slab case.

Further, we turn to examine the local flux distribution and its absolute error against the reference solution, shown in Fig. 3.15. The local error's magnitude confirms that the source convergence process could be accelerated with the low-order feedback and at Cycle 15, the

level of error in MC solution is approximately the same to that of the hybrid solvers. Since the convergence is again achieved immediately, assigning a factor of acceleration to either hybrid method is not meaningful but this confirms that even in continuous energy simulations, MC-FDSA can perform at a similar level to MC-CMFD in reducing the number of inactive cycles. Further, although the low-order feedback from MC-FDSA seems to fluctuate more severely than MC and MC-CMFD, the instability in convergence is not perturbed without any need of damping or manual manipulation of the process.

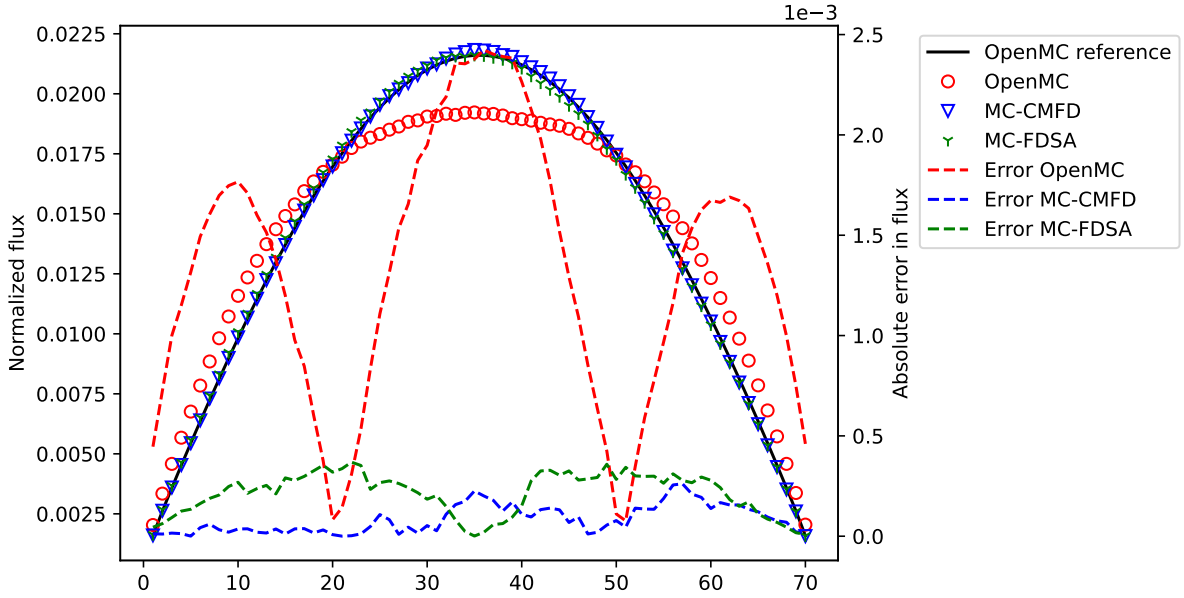

(a) Cycle 5.

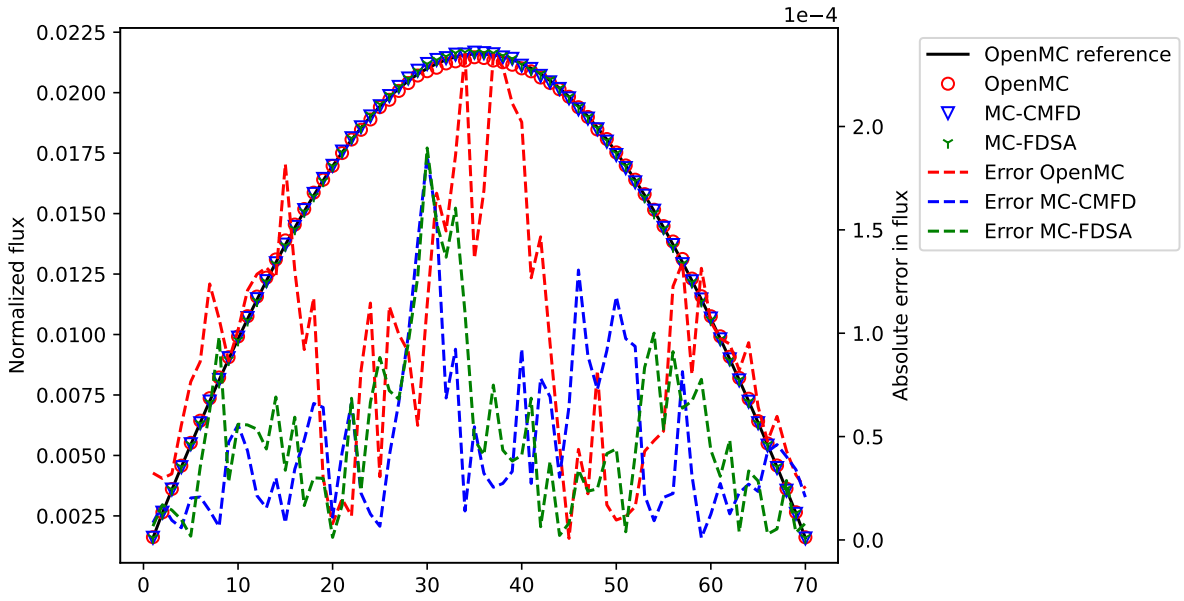

(b) Cycle 15.

Figure 3.15: Flux and absolute error in different cycles.

To demonstrate that the hybrid methods do not bring severe biases to the MC solution, the eigenvalues in the above cases are included in Table 3.6. No obvious deviation in eigenvalue

and its standard deviation could be observed for both hybrid solvers.

Table 3.6: Eigenvalues for the homogeneous slab case.

Solver	Eigenvalue
Ref	1.54854 ± 0.00001
OpenMC	1.54851 ± 0.00004
MC-CMFD	1.54853 ± 0.00004
MC-FDSA	1.54852 ± 0.00004

3.3.2 C5G7 full core simulation

The C5G7 benchmark [49] problem features a 16-assembly mini-core in 1/4 symmetry and simulation results have been completed with a vast collection of neutronics solvers with entirely different theoretical foundations. More conveniently all material compositions are provided in the benchmark for MC simulations alike and thus it is chosen as the endpoint example in our project. With these material compositions and the exact pin-resolved geometry including all fuel pins with double cladding, guide tubes, fission chambers and reflective regions, shown in Fig. 3.16, the benchmark problem is built with OpenMC.

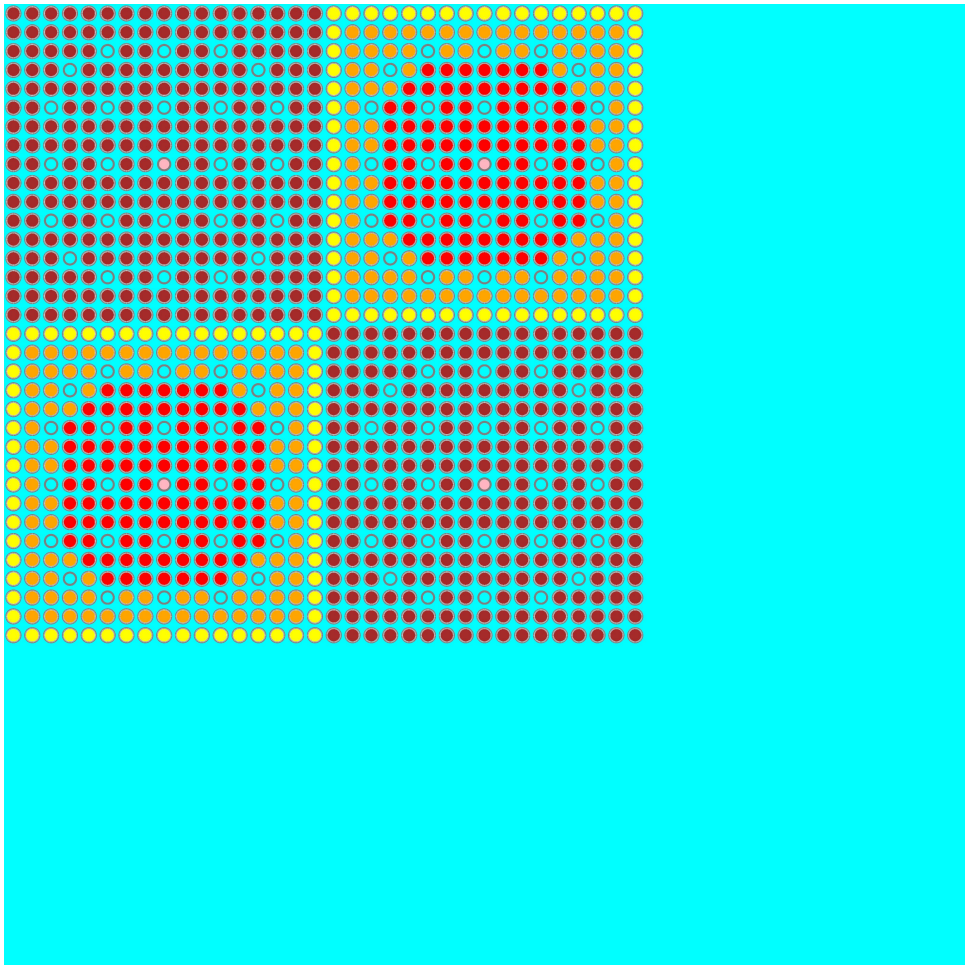

Figure 3.16: 2D configuration of C5G7 problem.

To determine the number of particles per cycle needed for accurate results for both the tallies and eigenvalues, we firstly conduct a sensitivity study on it and completed a series of tests with 200 (50 inactive) cycles in OpenMC. The eigenvalues and their standard deviations of these tests are shown in Table 3.7. Judging on the standard deviations in these cases, we see no significant benefits of increasing number of particles per cycle beyond 1 million. Further, in later tests we find that for the physical problem presented here, 1 million particles per cycle is sufficient to generate tallies that are accurate enough for the low-order problems in terms of accuracy in solution and convergence stability. Thus for all the following cases on the C5G7 benchmark 1

million particles per cycle with 50 inactive and 150 active cycles are used.

Table 3.7: Eigenvalues and Std Dev in sensitivity study.

Particles per cylce	k_{eff}	Std Dev in k_{eff}
100,000	1.17791	0.00022
1 million	1.17794	0.00008
2 million	1.17773	0.00006
5 million	1.17777	0.00004
10 million	1.17776	0.00002

As for the low-order problems, a uniform rectangle mesh, one cell for each pin, is used as no coarse mesh capability has been investigated yet. In terms of energy group structures, another sensitivity study is carried out for MC-FDSA as previous study [50] showed that MC-CMFD demonstrates no particular sensitivity towards the number of groups used in CMFD calculation. For MC-FDSA, we chose 1-group, 2-group from CASMO [51], 7-group, and 18-group [52] structures for the sensitivity study, in comparison against MC-CMFD with 7-group structure in CMFD. Fig. 3.17 shows the root mean square (RMS) of absolute error in fission source from cases with different energy groups in FDSA.

$$\sigma_\phi = \sqrt{\frac{1}{I}\sum_{i=1}^{I}\left(\phi_i - \phi_i^{Ref}\right)^2} \tag{3.1}$$

It could be seen that except the 1-group case, most cases could reduce the error in fission source faster than OpenMC, albeit at different rates. The 2-group case is slightly slower, converging at Cycle 8, while the 7-group and 18-group cases show a similar behavior to the

homogeneous slab case and converge almost immediately at Cycle 3. The 1-group case turns out to be quite troublesome in converging and due to the drastically changing group constants and eigenvalue at the beginning of the MC simulation, the 1-group FDSA feedback has to be delayed to Cycle 5 in order to achieve a stable convergence. Even so, it is still not converging faster than OpenMC.

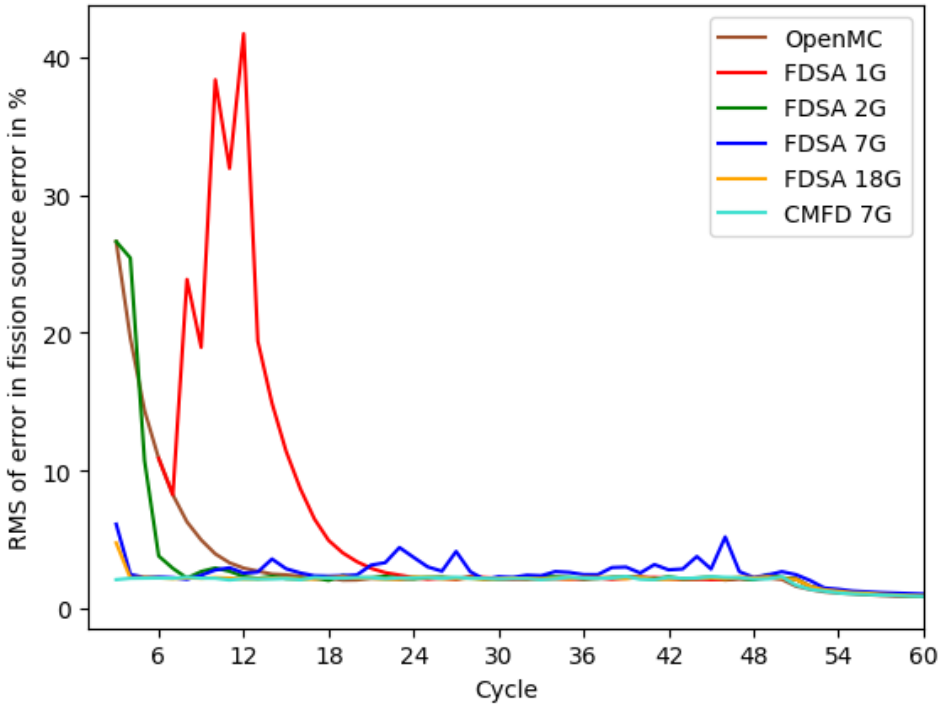

Figure 3.17: RMS of error in fission source in inactive cycles.

The Shannon entropy from these cases, plotted in Fig. 3.18, showed the same behavior in these cases among which the 7-group and 18-group cases are almost identical in the first few cycles. The 2-group case takes a few more cycles to converge and stabilize. The 1-group case is difficult to converge and heads to the wrong direction at the beginning but eventually arrives at the correct solution albeit slower than OpenMC.

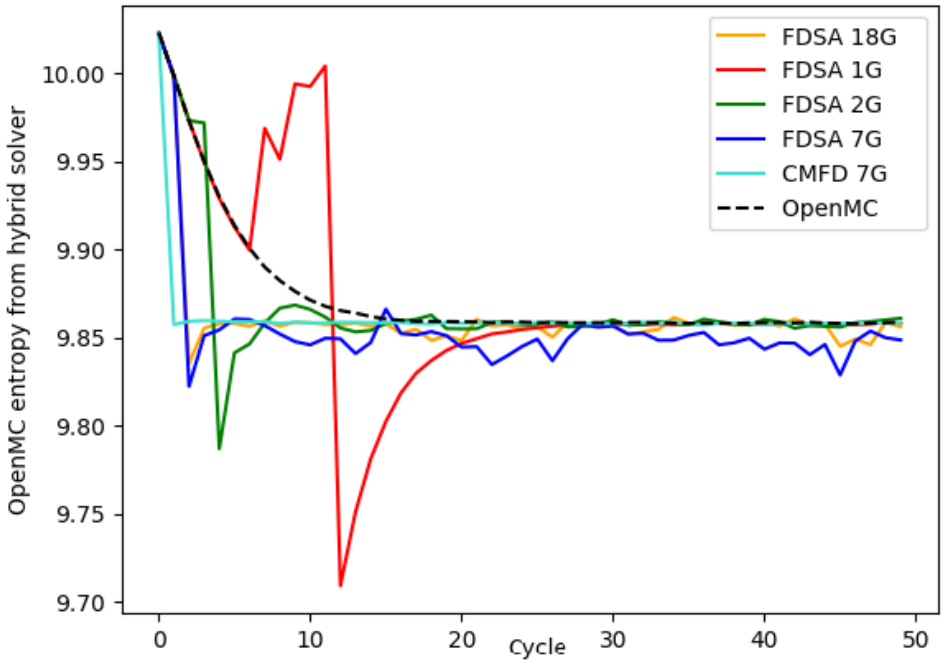

Figure 3.18: Shannon entropy in inactive cycles.

The eigenvalue in different cycles, plotted in Fig. 3.19 spans over the active cycles and shows that the differences in eigenvalues at the end of calculation are not as high as thought even though the 1-group case is not ideal at the beginning. For all cases, the error in eigenvalues ranges from 5 pcm to 50 pcm with the 18-group case being the closest to the reference solution. This is understandable due to the benefit of refined group structure. However, it is also observed that the 7-group case is surprisingly outperformed by the 2-group one.

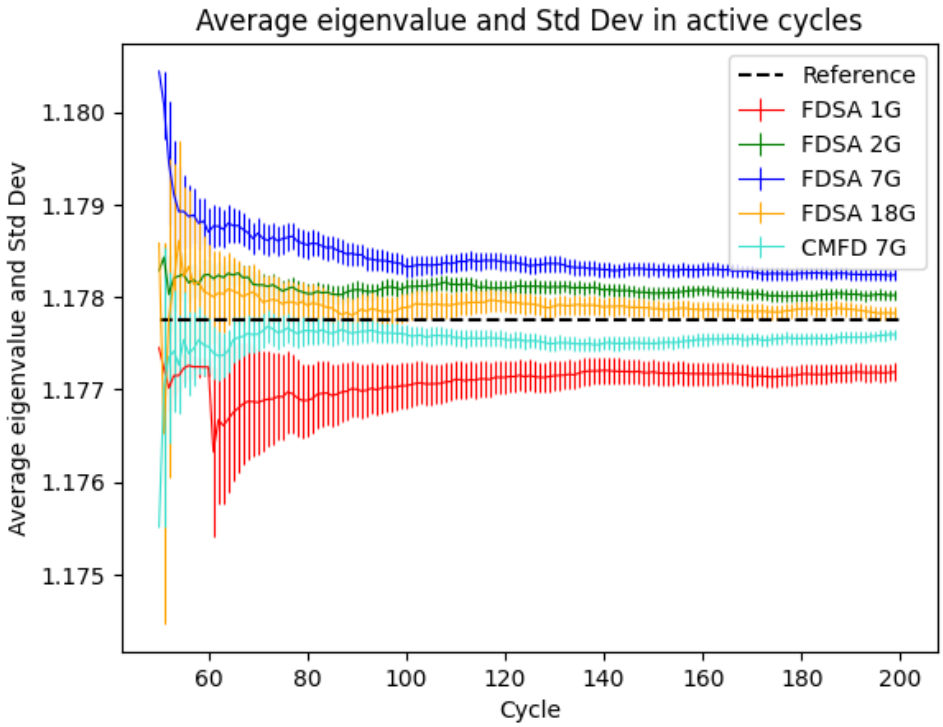

Figure 3.19: Eigenvalue against MC cycles.

The final eigenvalues and their standard deviations are gathered in Table 3.8. Again the end results are not severely biased by the use of MC-FDSA.

Table 3.8: Eigenvalues and standard deviations in C5G7 full-core cases.

Solver	Eigenvalue
Ref	1.17776 ± 0.00002
MC-FDSA 1G	1.17730 ± 0.00009
MC-FDSA 2G	1.17754 ± 0.00004
MC-FDSA 7G	1.17820 ± 0.00005
MC-FDSA 18G	1.17786 ± 0.00004
MC-CMFD 7G	1.17785 ± 0.00004

It has been shown by the above results that MC-FDSA could be applied in full-core realistic MC simulations and achieve similar performance to MC-CMFD without impacting the high-order transport calculations. It has also been found that in order to achieve the intended acceleration in source convergence, one needs to use sufficient number of particles per cycle to ensure accurate evaluation of group constants, and to choose adequate energy group structure, i.e. avoiding 1-group structure for MC-FDSA.

3.4 Comparison of FDSA against other methods

Unlike DSA, the FDSA method is developed specifically for acceleration of power iterations for solving eigenvalue problems. The inclusion of transport eigenvalues makes the FDSA low-order problem nonlinear which does not defeat the convergence stability entirely.

Previous FDSA includes the step of preconditioning with adjoint and forward diffusion solutions. Because of the gap between diffusion and transport solutions, previous FDSA method requires damping, or lessening, of the correction in order for the solution to converge. This significantly limits the versatility of FDSA and attaches the convergence stability of it to the choice of damping factors, which could only be determined empirically.

The FDSA method introduced here avoids the preconditioning step. Skipping this step provides three benefits: a) greatly improves the convergence stability to suit different physical problems, b) removes the necessity of damping or the search of adequate damping factors, c) simplifies the algorithm. At this moment a theoretical proof of FDSA's convergence stability is absent, yet the numerical experiments included in this chapter indicate that the method possesses a stable performance similar to other acceleration schemes in a wide range of applications.

In this work comparison is only made between FDSA and the popular CMFD. The completed tests demonstrate that FDSA behaves as intended as an acceleration scheme for power iterations. Its convergence behavior and structure are both similar to that of CMFD. However, because the low-order FDSA problem is not an eigenvalue problem, the reduction of transport calculations is less impressive than CMFD. This could be countered by the less solves of the low-order problem and the actual runtime of the two methods depends on the type of applications. Though the discretization for both methods is inconsistent with the transport equation's, FDSA arrived at solutions in good agreements with the transport solver, while CMFD would have a small deviation that would require tighter convergence criteria to minimize.

In cases done with the hybrid solvers, MC-FDSA performs better in achieving the source

convergence acceleration and becomes more competitive to MC-CMFD. In both the homogeneous slab case and C5G7 full core case, MC-FDSA is able to immediately converge the source distribution and provide stable low-order feedback without any manipulation. The converged solutions of these cases have good agreement with both MC-CMFD and the reference MC solutions without any obvious bias. Sensitivity study is carried out to examine the energy group structure in the low-order FDSA problem and its impact on the source convergence process, the converged solution's accuracy and convergence stability, the results of which demonstrate the effectiveness of MC-FDSA in acceleration of source convergence.

3.5 Summary

The numerical tests are conducted in the order of one-group and multigroup for both deterministic and stochastic methods with FDSA, and hybrid cases for homogeneous and full core calculations. To prove the concept of FDSA, simple one-group tests were conducted to ensure that the FDSA method possess stable convergence behavior with deterministic methods and is thus applicable to the construction of a hybrid MC-FDSA method. The one-group results indicate that FDSA, though not immediately comparable to CMFD, does function as intended. With its versatile algorithm regarding normalizations, the development of hybrid MC-FDSA method was fluid and the acceleration effect was present in the source convergence process in MC calculations. For the one-group heterogeneous problem in 1D tested here, FDSA could provide a speedup of about 15-20 in terms of number of transport calculations required for the deterministic methods, while the source convergence in hybrid solver could be accelerated by a factor of 15.

With the success of FDSA in one-group problems, the multigroup FDSA was then derived and implemented. The investigation of multigroup FDSA was conducted in the same manner as the one-group one, first in S_N solver and then in the hybrid solver. A 7-group 2-assembly test was constructed for a physical problem closer to the practical reactor application. The numerical results of this test show that the behavior of FDSA, both in convergence stability and acceleration effect, is similar to that in the one-group problem. Because the multigroup problem is much easier to solve, the extent to which the number of iterations could be reduced is limited. With FDSA the S_N solver could achieve convergence 60% faster, about 10% more transport iterations than CMFD. However, FDSA requires 40 times less iterations in the low-order problems for the problem, which brings the actual computational costs of the two methods to the same level for the 7-group problem. For the hybrid solver, FDSA is even more efficient and the source convergence is achieved almost instantly after the FDSA feedback is first applied.

The acceleration in the hybrid solver is about 10 times.

With the hybrid MC-FDSA solver, a homogeneous slab case with continuous energy cross section was first completed to demonstrate the feasibility of applying FDSA in a hybrid method. Later a C5G7 full core case was built with the goal of extending the method to more realistic applications. Both cases show good agreement between MC-FDSA, MC-CMFD and MC reference, with the conclusion that in various continuous energy MC simulations MC-FDSA's performance is as good as MC-CMFD for source convergence acceleration.

A comparison of FDSA against DSA, previous work on FDSA and CMFD explained the main differences, both theoretical and numerical ones, among these methods. FDSA, with its simplification and improved implementation approach, could reach the same level of acceleration and convergence stability required for the applications considered in this work.

CHAPTER

4

NUMERICAL RESULTS: VARIANCE REDUCTION

In extension to the hybrid solver's development, MC-FDSA is also applied to the active cycles in order to achieve variance reduction. This is in general done by applying the low-order feedback to MC fission source distribution with the same algorithm as shown in Chapter 2, with some adjustment in the algorithm. As introduced in Chapter 2, the apparent and real variances or their square roots are regarded as crucial estimators of the statistical error and should be compared between the hybrid and MC solvers. To accomplish this, we further investigate the three hybrid cases presented in Chapter 3 and evaluate the variances accordingly. In order to do so, each

one of these cases are repeated 20 times to obtain the independent results which lead to the computation of apparent and real variances, and also the real-to-apparent ratio.

4.1 Multigroup 2-assembly slab case

Due to the lack of a MC-CMFD solver for multigroup cases, only MC and MC-FDSA are compared here. The apparent and real standard deviations (SD) of the flux in 1st group are computed and plotted in Fig. 4.1.

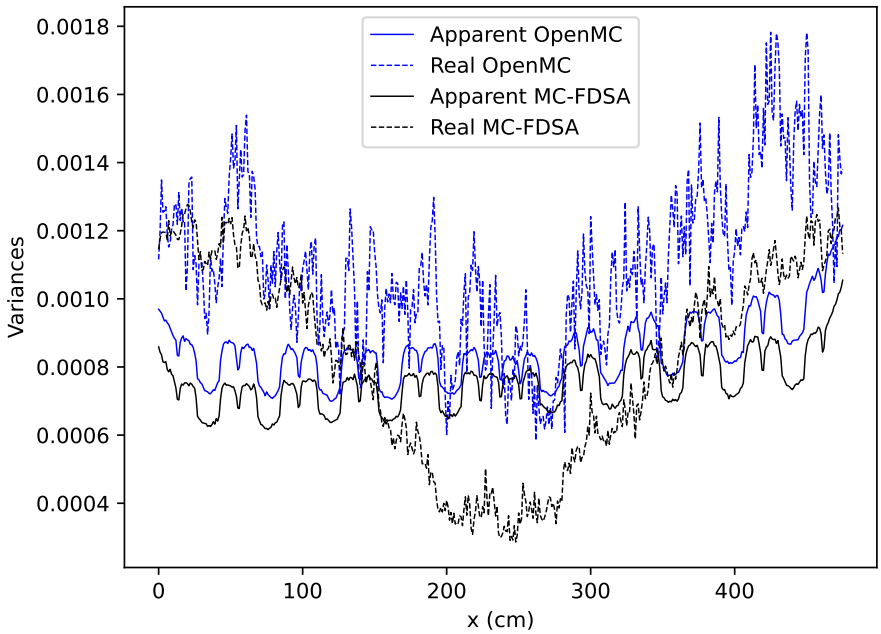

Figure 4.1: Real and apparent Std Dev of normalized flux in 1st group.

The apparent SD in MC-FDSA is uniformly 15-20% smaller than that in MC, while the real SD in MC-FDSA does not display this behavior, but instead shows a more significant reduction in the middle of the geometry. This could be attributed to the direct treatment of boundary condition in the multigroup solver instead of an albedo boundary condition evaluated with MC

tally. Overall the real SD in MC-CMFD is even smaller than that in MC. To illustrate how much reduction is achieved from apparent SD to real SD, the real-to-apparent ratio is shown in Fig. 4.2.

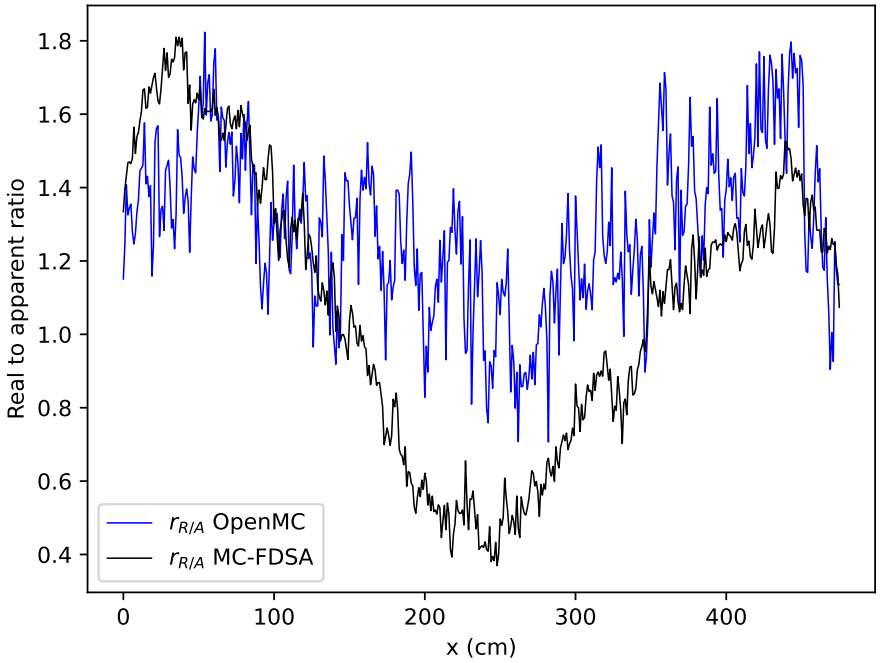

Figure 4.2: Real to apparent ratio of normalized flux in 1st group.

In general the real-to-apparent ratio in MC-FDSA is lower than that in MC, indicating that the variance reduction is achieved. Comparing this to the previous work on MC-CMFD [32, 53], it could be found that the real-to-apparent ratio in MC-FDSA is not as high and the real SD does not equal or land close to the apparent SD like it does for MC-CMFD. These results of course depend on the physical problems and should not be considered universal. With results from MC-CMFD in the continuous energy cases, we should have a better understanding on this.

4.2 Continuous energy homogeneous slab case

For the continuous energy cases, the computation of cross sections depends on the MC tallies which in active cycles are accumulated and averaged, hence the tallies are not reset at each cycle. This leads to the necessity of a damping factor d as mentioned in Chapter 2 on the FDSA correction terms to avoid negative fluxes, which often occur at a few cycles after the accumulation of tallies starts. The benefit of accumulated tallies is that the cross sections used in FDSA and CMFD are more "stable" and thus one should expect less convergence instability. The apparent and real SDs from MC, MC-CMFD and MC-FDSA are computed at the end of the 150 active cycles and shown in Fig. 4.3.

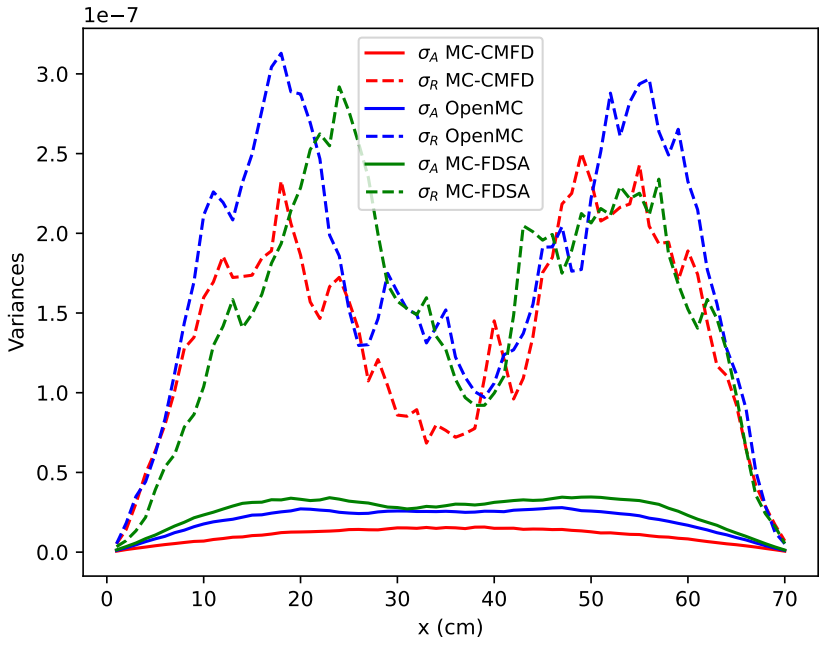

Figure 4.3: Real and apparent Std Dev of normalized flux.

For the continuous energy case, the behaviors of both apparent and real SDs are different from those in the multigroup case. The real SD is much higher than the apparent SD for all

three solvers and the MC-CMFD and MC-FDSA ones are smaller than the MC one overall. The apparent SD in MC-FDSA is on the contrary larger than that in MC although not by a large margin. On the other hand, the MC-CMFD SDs are both smaller than MC SDs respectively. Since real SD is closer to the true variances in MC methods, MC-FDSA and MC-CMFD could be both regarded as successful in reducing the variances at a rate similar to what was found in continuous energy cases in previous work on MC-CMFD [53]. The real-to-apparent ratio can be computed with these SDs and plotted in Fig. 4.4. Because of the smaller values of σ_A in MC-FDSA, $r_{R/A}$ is the largest for MC-CMFD while the one for MC-FDSA is the smallest.

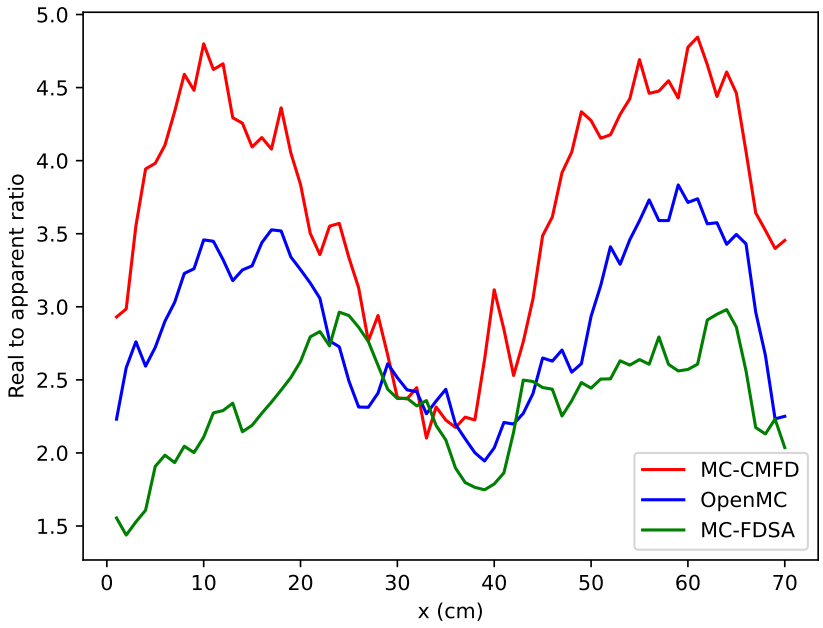

Figure 4.4: Real to apparent ratio of normalized flux.

4.3 Continuous energy C5G7 full core case

For the variance reduction in active cycles, the real and apparent SDs of pin-by-pin fission source are computed at the end of Cycle 200 and plotted in Fig. 4.5. Overall it shows no obvious differences in either real or apparent SD among all 3 solvers. To evaluate the distribution of variances in terms of magnitude, the SDs are cast into histograms shown in Fig. 4.5.

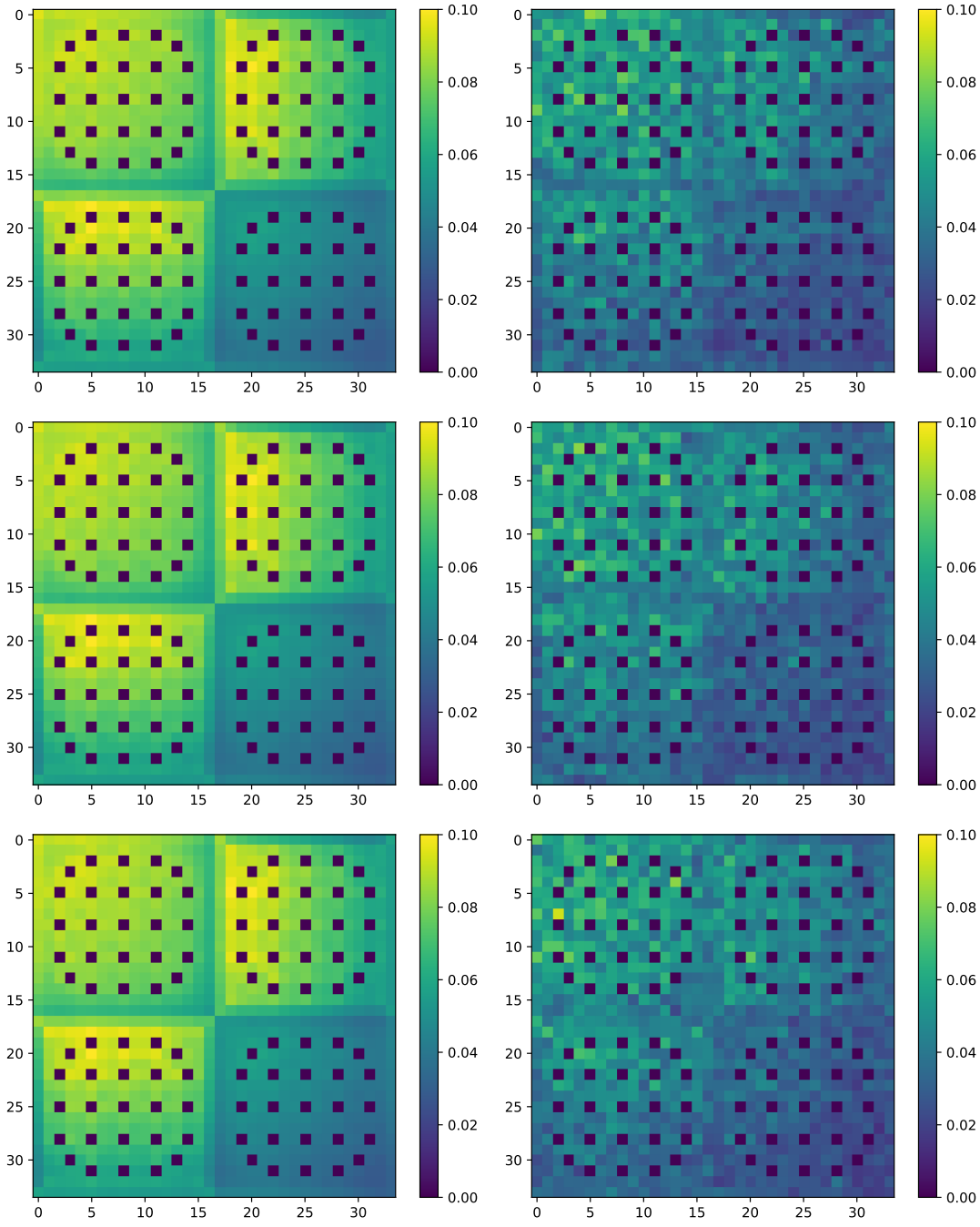

Figure 4.5: Apparent (1st column) and real (2nd column) SDs of fission source from OpenMC, MC-CMFD and MC-FDSA (from top to bottom respectively).

Excluding the guide tube cells where fission source is zero, most of the MC tallies on fission

source include some levels of statistical error as shown in Fig. 4.6a. Compared to the apparent SD, the real SD is reduced by all 3 solvers at almost identical rates. Compared to what is observed in the homogeneous slab test and work by Park et al [41], these results suggest that for systems with smaller physical dimensions, i.e., smaller dominance ratio, the effect of variance reduction is limited for this type of hybrid neutronics method.

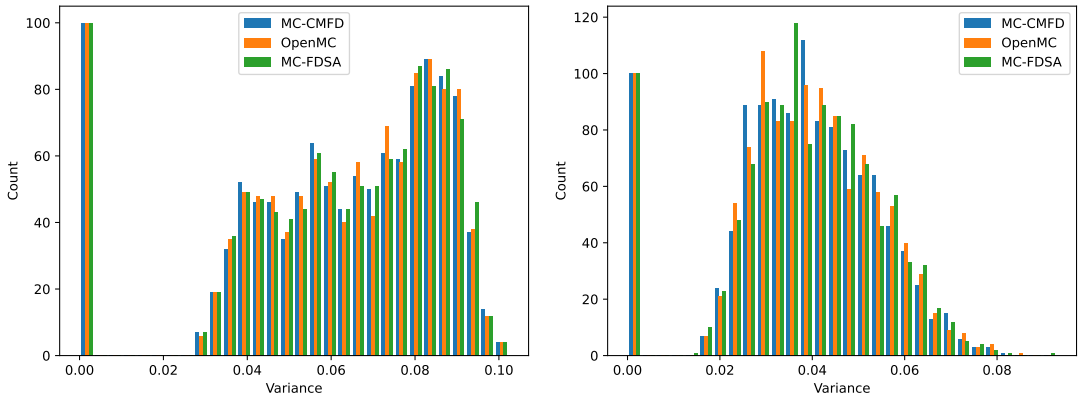

(a) Apparent SDs.

(b) Real SDs.

Figure 4.6: Histograms of real and apparent SDs.

4.4 Summary

In this chapter, we compared the real and apparent variances in three cases completed with the hybrid solvers, aiming to evaluate the variance reduction capability in MC-FDSA. For the multigroup heterogeneous slab case, a 15-20% reduction in real variance could be seen with MC-FDSA against MC, and because there is no result from MC-CMFD available, no baseline is established for our method.

In the continuous energy cases MC, MC-CMFD and MC-FDSA were directly compared against each other. In the homogeneous slab case, although MC-FDSA is able to reduce the real variance at a rate close to that in MC-CMFD, the apparent variance in MC-FDSA is on the contrary higher than the MC one. The MC-CMFD results in this case are close to previous work on MC-CMFD and while not entirely satisfying, we found MC-FDSA to be able to reduce at least the real variance in MC.

The same conclusion cannot be made with the C5G7 full core calculation, as the real and apparent variances in both MC-CMFD and MC-FDSA do not display any significant diminution from the MC ones. For systems with a small dominance ratio like this, the hybrid methods' effectiveness in variance reduction is limited and thus we could not properly evaluate MC-FDSA in this case.

CHAPTER

5

CONCLUSIONS AND FUTURE WORK

5.1 Conclusions

This PhD research project aims at developing a novel FDSA scheme for k-eigenvalue problems suitable for both deterministic and stochastic neutronics methods, with a focus on hybrid neutronics method for source convergence acceleration and variance reduction. The scope of this work covers the theoretical, numerically experimental and algorithmic development of FDSA.

The novel FDSA was created to address issues in previous work that originates from the preconditioning with adjoint and forward diffusion solutions. In physical problems that includes drastic transport effect of neutrons, previous FDSA method would provide corrections that

deviate from the transport solution towards the diffusion one, which led to the undesired convergence instability. Solution to this instability was to apply a damping factor, which displays no physical pattern and is determined empirically, onto the corrections. The novel FDSA circumvents the preconditioning step and fixates the eigenfunction and eigenvalue of neutron fluxes directly with the transport solutions. The mathematical proof of such a concept is absent, yet the benefits of it prodded the author to develop numerically a new acceleration method for k-eigenvalue problem.

The proof of concept was firstly accomplished by the derivation of one-group one-dimensional FDSA which was later implemented in a S_N solver and tested with referenced cases from previous work. The novel FDSA method was shown to be able to achieve stable convergence and to provide the desired acceleration for deterministic calculations. This laid foundation for the development of a hybrid MC-FDSA solver and the implementation of FDSA as an external module of OpenMC accomplished this task. The MC-FDSA solver, in the same tests on S_N solver, demonstrated similar convergence behavior and accelerates the source convergence process in MC calculation, significantly lowering the number of inactive cycles required. The success of FDSA in one-group problem led to the multigroup generalization, the investigation of which yielded similar results with a test modified from the C5G7-TD benchmark[49]. This test was designed with the purpose to imitate realistic reactor criticality calculations. As expected, both the deterministic and hybrid FDSA solvers were able to accelerate the transport calculations without impacting the convergence stability or accuracy. Moreover, the comparison with CMFD in the multigroup case showed that the novel FDSA is comparable to contemporary acceleration methods.

Later the hybrid MC-FDSA is implemented for continuous energy MC simulations as well and several tests were constructed to complete validation and verification, and to demonstrate MC-FDSA's capabilities in handling continuous energy cross sections. The algorithm and implementation strategy of MC-FDSA in continuous energy range was similar to MC-CMFD

and these two methods were compared side by side in two cases, a homogeneous slab with artificial material composition and C5G7 full core case. The acceleration of source convergence in these cases could be instantly achieved with MC-FDSA which is on par with MC-CMFD, and the convergence process was stable without further manipulation as in the multigroup case. On the issue of variance reduction, only mixed results were obtained. The multigroup case showed that the variance reduction could be achieved with MC-FDSA by a factor of 2, which is not as drastic as previous work on MC-CMFD in multigroup range. As for the continuous energy cases, MC-FDSA can reduce the real variance by about 20% like MC-CMFD in the same case. However, such performance could not be observed in the C5G7 full core case for both MC-FDSA and MC-CMFD, which indicated that the hybrid neutronics method might not be effective in variance reduction for systems with low dominance ratio.

5.2 Future work

What is covered in this thesis is in no way exhaustive of the MC-FDSA method itself or related work on hybrid neutronics method. On optimizing and extending MC-FDSA to a wider range of applications, further investigation is needed in different MC tally averaging scheme in both inactive and active cycles and their impacts on the hybrid neutronics method, as we have seen the sensitivity of MC-FDSA and MC-CMFD to the group constants computed with these MC tallies in terms of convergence stability and accuracy of feedback. Taking into the account the effects of low-order feedback on the variances in the active cycles, two different strategies should be taken for inactive and active cycles and adjust the algorithm of the hybrid solvers accordingly.

Since the C5G7 full core case is not physically difficult enough in order to demonstrate the effectiveness of MC-FDSA in variance reduction, a larger PWR model is needed. To complete the set of MC and MC-FDSA simulations, one would be faced with an exceedingly large system of equations in the low-order FDSA problem if the pin mesh is used. Thus the investigation of coarse mesh capability in MC-FDSA is also crucial to applying the method in realistic scenarios.

Another crucial component of this study is the investigation of biases brought by the spatial and energy discretization in the low-order FDSA problem on the MC solution. A mesh refinement study in the low-order problem with the same geometry in MC modeling would be sufficient to quantify the biases on both the local variables such as fission source and the eigenvalue.

A mathematical proof of the convergence in FDSA to the transport solution is also missing which to some might be crucial in the applicability of such a method. Further, a stability analysis on FDSA in deterministic method and MC-FDSA with linearization and Fourier analysis for further investigation on their respective application ranges.

Lastly, although not pursued in this project due to the focus on hybrid neutronics method,

the FDSA method might be used in conjunction with other methods such as DSA and CMFD to construct multilevel iterative schemes that could prove to be more advantageous towards the method itself. And further applications could be developed in hybrid neutronics methods in the same way FDSA was developed first in deterministic method and then in hybrid methods.

REFERENCES

[1] Dmitri Yu Anistratov and Vladimir Ya Gol'Din. Nonlinear methods for solving particle transport problems. *Transport Theory and Statistical Physics*, 22(2-3):125–163, 1993.

[2] Marvin L Adams and Edward W Larsen. Fast iterative methods for discrete-ordinates particle transport calculations. *Progress in nuclear energy*, 40(1):3–159, 2002.

[3] Dmitriy Y Anistratov and Vladimir Ya Gol'din. Multilevel quasidiffusion methods for solving multigroup neutron transport k-eigenvalue problems in one-dimensional slab geometry. *Nuclear science and engineering*, 169(2):111–132, 2011.

[4] Luke R Cornejo, Dmitriy Y Anistratov, and Kord Smith. Iteration methods with multigrid in energy for eigenvalue neutron diffusion problems. *Nuclear Science and Engineering*, 193(8):803–827, 2019.

[5] Kord S Smith. Full-core, 2-d, lwr core calculations with casmo-4e. *PHYSOR 2002, Seoul, Korea*, 2002.

[6] Nam-Zin Cho, GS Lee, and CJ Park. Partial current-based cmfd acceleration of the 2d/1d fusion method for 3d whole-core transport calculations. *Transactions of the American Nuclear Society*, 88:594–594, 2003.

[7] Dmitriy Y Anistratov. Multilevel nda methods for solving multigroup eigenvalue neutron transport problems. *Nuclear Science and Engineering*, 174(2):150–162, 2013.

[8] Luke R Cornejo and Dmitriy Y Anistratov. The multilevel quasidiffusion method with multigrid in energy for eigenvalue transport problems. *Progress in Nuclear Energy*, 101: 401–408, 2017.

[9] Ben C Yee, Brendan Kochunas, and Edward W Larsen. A multilevel in space and energy solver for multigroup diffusion eigenvalue problems. *Nuclear Engineering and Technology*, 49(6):1125–1134, 2017.

[10] Guangchun Zhang, Albert Hsieh, Won Sik Yang, and Yeon Sang Jung. Consistent pcmfd acceleration schemes of the three-dimensional transport code proteus-moc. *Nuclear Science and Engineering*, 193(8):828–853, 2019.

[11] Dean Wang, Thomas Downar, Yunlin Xu, Yulong Xing, and Emily Shemon. Development of a novel accelerator for neutron transport solution using the galerkin spectral element methods. Technical report, Univ. of Massachusetts, Lowell, MA (United States), 2019.

[12] Edward W Larsen and Blake W Kelley. The relationship between the coarse-mesh finite difference and the coarse-mesh diffusion synthetic acceleration methods. *Nuclear Science and Engineering*, 178(1):1–15, 2014.

[13] Raymond E Alcouffe. Diffusion synthetic acceleration methods for the diamond-differenced discrete-ordinates equations. *Nuclear Science and Engineering*, 64(2):344–355, 1977.

[14] Edward W Larsen. Unconditionally stable diffusion-synthetic acceleration methods for the slab geometry discrete ordinates equations. part i: Theory. *Nuclear Science and Engineering*, 82(1):47–63, 1982.

[15] François Févotte. Piecewise diffusion synthetic acceleration scheme for neutron transport simulations in optically thick systems. *Annals of Nuclear Energy*, 118:71–80, 2018.

[16] Todd James Urbatsch. Iterative acceleration methods for monte carlo and deterministic criticality calculations. Technical report, Los Alamos National Lab., NM (United States), 1995.

[17] Taro Ueki. Information theory and undersampling diagnostics for monte carlo simulation of nuclear criticality. *Nuclear science and engineering*, 151(3):283–292, 2005.

[18] Taro Ueki and Forrest B Brown. Stationarity modeling and informatics-based diagnostics in monte carlo criticality calculations. *Nuclear science and engineering*, 149(1):38–50, 2005.

[19] Forrest B Brown. On the use of shannon entropy of the fission distribution for assessing convergence of monte carlo criticality calculations. In *ANS topical meeting on reactor physics (PHYSOR 2006). Canadian Nuclear Society, Canada*, 2006.

[20] Qiong Zhang and Hany S Abdel-Khalik. Global variance reduction for monte carlo reactor physics calculations. In *Proceedings of the 2013 International Conference on Mathematics and Computational Methods Applied to Nuclear Science and Engineering-M and C 2013*, 2013.

[21] John C Wagner, Edward D Blakeman, and Douglas E Peplow. Forward-weighted cadis method for global variance reduction. *Transactions-American Nuclear Society*, 97:630, 2007.

[22] Jaakko Leppänen and Mika Jokipii. Global variance reduction scheme with self-adaptive weight-window mesh in the serpent 2 monte carlo code. In *International Conference on Mathematics and Computational Methods applied to Nuclear Science and Engineering*, pages 85–95. American Nuclear Society ANS, 2019.

[23] Kenneth W Burn. Optimizing variance reduction in monte carlo eigenvalue calculations that employ the source iteration approach. *Annals of Nuclear Energy*, 73:218–240, 2014.

[24] Marc A Cooper and Edward W Larsen. Automated weight windows for global monte carlo particle transport calculations. *Nuclear science and engineering*, 137(1):1–13, 2001.

[25] Edward W Larsen and Jinan Yang. A functional monte carlo method for k-eigenvalue problems. *Nuclear Science and Engineering*, 159(2):107–126, 2008.

[26] Bethany R Robinson. Investigation of a hybrid quasi-diffusion/monte carlo method for solving multigroup criticality problems in slab geometry. 2011.

[27] Han Dong, Mahesh Ravishankar, Paul Sathre, Michael B Sullivan, William Taitano, Jeffery Willert, Tim Germann, Dana Knoll, Bryan Lally, Pat McCormick, et al. Quasi diffusion accelerated monte carlo. *Los Alamos National Laboratory*, 2011.

[28] Min Jae Lee, Han Gyu Joo, Deok Jung Lee, and Kord Smith. A feasibility study of cmfd acceleration in monte carlo eigenvalue calculation. 2009.

[29] Min-Jae Lee, Han Gyu Joo, Deokjung Lee, and Kord Smith. Investigation of cmfd accelerated monte carlo eigenvalue calculation with simplified low dimensional multigroup formulation. *Proc. PHYSOR 2010*, pages 9–14, 2010.

[30] Min-Jae Lee, Han Gyu Joo, Deokjung Lee, and Kord Smith. Multigroup monte carlo reactor calculation with coarse mesh finite difference formulation for real variance reduction. In *Joint International Conference on Supercomputing in nuclear Applications and Monte Carlo*, pages 17–21, 2010.

[31] Sunghwan Yun and Nam Zin Cho. Acceleration of source convergence in monte carlo k-eigenvalue problems via anchoring with a p-cmfd deterministic method. *Annals of Nuclear Energy*, 37(12):1649–1658, 2010.

[32] Emily R Wolters, Edward W Larsen, and William R Martin. Generalized hybrid monte carlo-cmfd methods for fission source convergence. 2011.

[33] Jeffrey Willert, CT Kelley, Dana A Knoll, and H Park. Hybrid deterministic/monte carlo neutronics. *SIAM Journal on Scientific Computing*, 35(5):S62–S83, 2013.

[34] Lulu Li et al. *Acceleration methods for Monte Carlo particle transport simulations*. PhD thesis, Massachusetts Institute of Technology, 2017.

[35] Kendra P Keady and Edward W Larsen. Stability of monte carlo k-eigenvalue simulations with cmfd feedback. *Journal of Computational Physics*, 321:947–964, 2016.

[36] Bryan Robert Herman. *Monte Carlo and thermal hydraulic coupling using low-order nonlinear diffusion acceleration*. PhD thesis, Massachusetts Institute of Technology, 2014.

[37] Paul K Romano, Nicholas E Horelik, Bryan R Herman, Adam G Nelson, Benoit Forget, and Kord Smith. Openmc: A state-of-the-art monte carlo code for research and development. *Annals of Nuclear Energy*, 82:90–97, 2015.

[38] John C Wagner, Douglas E Peplow, and Scott W Mosher. Fw-cadis method for global and regional variance reduction of monte carlo radiation transport calculations. *Nuclear Science and Engineering*, 176(1):37–57, 2014.

[39] Jaakko Leppänen, Tuomas Viitanen, and Olli Hyvönen. Development of a variance reduction scheme in the serpent 2 monte carlo code. In *International Conference on Mathematics and Computational Methods Applied to Nuclear Science and Engineering, M&C 2017*, 2017.

[40] Min Jae Lee, Han Gyu Joo, Deokjung Lee, and Kord Smith. Coarse mesh finite difference formulation for accelerated monte carlo eigenvalue calculation. *Annals of Nuclear Energy*, 65:101–113, 2014.

[41] Jinsu Park, Peng Zhang, Hyunsuk Lee, Sooyoung Choi, Jiankai Yu, and Deokjung Lee. Performance evaluation of cmfd on inter-cycle correlation reduction of monte carlo simulation. *Computer Physics Communications*, 235:111–119, 2019.

[42] Jiahao Chen and Jason Hou. A hybrid neutronics method with diffusion synthetic acceleration for k-eigenvalue problem. *Transactions*, 122(1):417–420, 2020.

[43] Forrest B Brown. A review of monte carlo criticality calculations-convergence, bias, statistics. 2008.

[44] Taro Ueki. Intergenerational correlation in monte carlo k-eigenvalue calculation. *Nuclear science and engineering*, 141(2):101–110, 2002.

[45] Hyung Jin Shim and Chang Hyo Kim. Real variance estimation using an intercycle fission source correlation for monte carlo eigenvalue calculations. *Nuclear Science and Engineering*, 162(1):98–108, 2009.

[46] YuGwon Jo and Nam Zin Cho. Acceleration and real variance reduction in continuous-energy monte carlo whole-core calculation via p-cmfd feedback. *Nuclear Science and Engineering*, 189(1):26–40, 2018.

[47] Alain Hébert. *Applied reactor physics*. Presses inter Polytechnique, 2009.

[48] Jeffrey S Racine. A primer on regression splines. *URL: http://cranrprojectorg/web/packages/crs/vignettes/splineprimerpdf*, 2014.

[49] Jason Jia Hou, Kostadin N Ivanov, Victor F Boyarinov, and Peter A Fomichenko. Oecd/nea benchmark for time-dependent neutron transport calculations without spatial homogenization. *Nuclear Engineering and Design*, 317:177–189, 2017.

[50] Samuel Christopher Shaner. *Development of high fidelity methods for 3D Monte Carlo transient analysis of nuclear reactors*. PhD thesis, Massachusetts Institute of Technology, 2018.

[51] Joel Rhodes, Kord Smith, and Deokjung Lee. Casmo-5 development and applications. In *Proceedings of the PHYSOR-2006 conference, ANS Topical Meeting on Reactor Physics (Vancouver, BC, Canada, 2006) B*, volume 144, 2006.

[52] A Seubert, S Langenbuch, and W Zwermann. Status and development of nuclear design and accident simulation methods “, 2005.

[53] Hyunsuk Lee and Deokjung Lee. Application of cmfd on continuous energy monte carlo simulation for eigenvalue problems. *Trans. Kor. Nucl. Soc*, pages 29–31, 2014.

[54] Hans G Kaper, Arthur J Lindeman, and Gary K Leaf. Benchmark values for the slab and sphere criticality problem in one-group neutron transport theory. *Nuclear Science and Engineering*, 54(1):94–99, 1974.

APPENDICES

APPENDIX

A

DERIVATIONS

The derivation of the one-group FDSA equation is included in this section. This formulation was the first attempt of devising such a method in the proof of concept with an S_N solver. The self-adjoint fission and scattering sources in the one-group equations make the discretization of FDSA equation consistent to the high-order problem easier and the implementation of the formulation here led to the one-group deterministic results in Chapter 3.

A.1 Formulation of one-speed FDSA

Starting from the standard one-group transport equation in slab geometry, we have:

$$\mu \frac{\partial \psi(x,\mu)}{\partial x} + \Sigma_t(x)\psi(x,\mu) = \frac{1}{2}\Sigma_s(x)\phi(x) + \frac{\nu\Sigma_f(x)}{2k}\phi(x) \ , \tag{A.1}$$

where $\phi = \int_{-1}^{1} \psi d\mu$. Omit the dependencies and add indices for iterations:

$$\mu \frac{\partial \psi^{(l+1/2)}}{\partial x} + \Sigma_t \psi^{(l+1/2)} = \frac{1}{2}\Sigma_s \phi(x)^{(l)} + \frac{\nu\Sigma_f}{2k^{(l)}}\phi^{(l)} \ , \tag{A.2}$$

where l denotes the previous iteration and $l+1/2$ denotes the next iteration.

For transport calculation we equate $\psi^{(l+1)} = \psi^{(l+1/2)}$ and move to the next iteration. In the acceleration scheme we define the correction term as

$$g^{(l+1)} = \psi - \psi^{(l+1/2)} \ , \tag{A.3}$$

where ψ is the true solution to the transport equation, and the intermediate step is completed with

$$\psi^{(l+1)} = \psi^{(l+1/2)} + g^{(l+1)} \ . \tag{A.4}$$

Replace the true solution ψ and ϕ in Eq. (A.1) with Eq. (A.3)

$$\mu \frac{\partial \left(\psi^{(l+1/2)} + g^{(l+1)}\right)}{\partial x} + \Sigma_t \left(\psi^{(l+1/2)} + g^{(l+1)}\right) = \frac{1}{2}\Sigma_s \phi^{(l)} + \frac{\nu\Sigma_f}{2k}\left(\phi^{(l+1/2)} + \int_{-1}^{1} g^{(l+1)} d\mu\right) \ . \tag{A.5}$$

Subtract Eq. (A.2) from Eq. (A.5) and rearrange

$$\mu\frac{\partial g^{(l+1)}}{\partial x}+\Sigma_t g^{(l+1)}-\frac{1}{2}\Sigma_s\int_{-1}^{1}g^{(l+1)}d\mu-\frac{\nu\Sigma_f}{2k}\int_{-1}^{1}g^{(l+1)}d\mu= \frac{\nu\Sigma_f}{2k}\phi^{(l+1/2)}-\frac{\nu\Sigma_f}{2k^{(l)}}\phi^{(l)}\ . \quad \text{(A.6)}$$

Define the correction terms on scalar flux and current

$$f_0^{(l+1)}=\int_{-1}^{1}g^{(l+1)}d\mu\ , \quad \text{(A.7)}$$

$$f_1^{(l+1)}=\int_{-1}^{1}\mu g^{(l+1)}d\mu\ , \quad \text{(A.8)}$$

and substitute $\int_{-1}^{1}g^{(l+1)}d\mu$ in the previous equation:

$$\mu\frac{\partial g^{(l+1)}}{x}+\Sigma_t g^{(l+1)}-\frac{1}{2}\Sigma_s f_0^{(l+1)}-\frac{\nu\Sigma_f}{2k}f_0^{(l+1)}=\frac{\nu\Sigma_f}{2k}\phi^{(l+1/2)}-\frac{\nu\Sigma_f}{2k^{(l)}}\phi^{(l)}\ . \quad \text{(A.9)}$$

Apply operator $\int_{-1}^{1}\cdot d\mu$ on Eq. (A.9):

$$\frac{\partial f_1^{(l+1)}}{x}+\Sigma_t f_0^{(l+1)}-\Sigma_s f_0^{(l+1)}-\frac{\nu\Sigma_f}{k}f_0^{(l+1)}=\frac{\nu\Sigma_f}{k}\phi^{(l+1/2)}-\frac{\nu\Sigma_f}{k^{(l)}}\phi^{(l)}\ . \quad \text{(A.10)}$$

Apply operator $\int_{-1}^{1}\mu\cdot d\mu$ on Eq. (A.9):

$$\frac{\partial}{\partial x}\int_{-1}^{1}\mu^2 g^{(l+1)}d\mu+\Sigma_t f_1^{(l+1)}=0\ . \quad \text{(A.11)}$$

Apply the P1 approximation on the correction term $g^{(l+1/2)}$

$$g^{(l+1)}\approx\frac{1}{2}\left(f_0^{(l+1)}+3\mu f_1^{(l+1)}\right)\ , \quad \text{(A.12)}$$

and substitute in Eq. (A.11):

$$f_1^{(l+1)} = -\frac{1}{3\Sigma_t}\frac{\partial}{\partial x} f_0^{(l+1)} \ . \tag{A.13}$$

Substitute Eq. (A.13) into Eq. (A.10), and we have:

$$-\frac{\partial}{\partial x}\frac{1}{3\Sigma_t}\frac{\partial}{\partial x} f_0^{(l+1)} + \Sigma_t f_0^{(l+1)} - \Sigma_s f_0^{(l+1)} - \frac{\nu\Sigma_f}{k^{(l+1/2)}} f_0^{(l+1)} = \frac{\nu\Sigma_f}{k^{(l+1/2)}}\phi^{(l+1/2)} - \frac{\nu\Sigma_f}{k^{(l)}}\phi^{(l)} \ . \tag{A.14}$$

The correction term $f_0^{(l+1/2)}$ is applied to scalar flux by

$$\phi^{(l+1)} = \phi^{(l+1/2)} + f_0^{(l+1)} \ , \tag{A.15}$$

and the new eigenvalue is evaluated with

$$k^{(l+1)} = k^{(l+1/2)} \frac{\int \nu\Sigma_f \phi^{(l+1)} dx}{\int \nu\Sigma_f \phi^{(l+1/2)} dx} \ . \tag{A.16}$$

The low-order FDSA problem consists of Eq. (A.14),(A.15) and (A.16).

APPENDIX

B

MISCELLANEOUS NUMERICAL RESULTS

B.1 MC-DSA tests

In the study of hybrid MC-DSA method [42], we used a one-group homogeneous eigenvalue problem in slab geometry for testing.

The homogeneous slab has reflective boundary condition on the left side and vacuum boundary condition on the right side. It has width of 30 cm, with artificial cross section $\Sigma_t = 1.0$ cm^{-1}, $\Sigma_s = 0.7$ cm^{-1}, and $\nu\Sigma_f = 0.3071$ cm^{-1} from the benchmark[54]. A uniform

mesh of 30 cells, each 1 cm thick is used for modeling the geometry in OpenMC and DSA discretization. The reference k_{eff} is 1.02076 ± 0.00006, calculated by OpenMC with 50,000 particles per cycle and 5,000 cycles (1,000 inactive cycles), while an S_N solution with S_{32} quadrature set and same spatial mesh is 1.02082. All the following results will regard the OpenMC case as reference. For the rest of the testing results, the OpenMC case will be regarded as the reference.

The OpenMC calculation, starting with a uniform source distribution, uses 50,000 particles per cycle and the source distribution converges around 1,400th cycle.

The DSA feedback is turned on at the second cycle since two consecutive cycles are needed to generate the inputs for the DSA module. This is not to say that DSA has to be started at the beginning of the calculation, but the effect of starting DSA at some point later is not investigated. To check whether the accelerated OpenMC solution is improved by the DSA feedback towards an incorrect source distribution, this case is run for 1,000 cycles and the flux distribution is checked at different cycles, shown in Fig. B.1. The reference solution and the unaccelerated OpenMC solutions at different cycles are also included in the same figure. The flux distribution with the DSA feedback, shown in solid lines converges much faster than the unaccelerated flux shown in dotted lines.

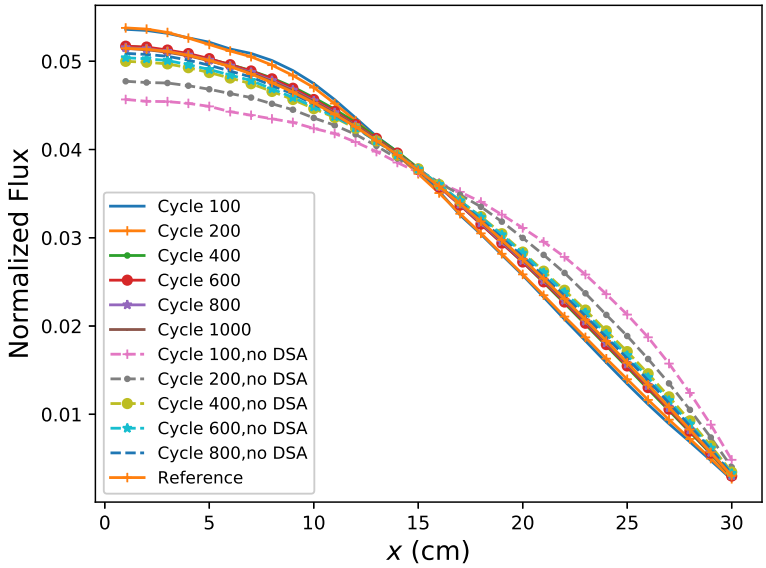

Figure B.1: Normalized flux at different cycles with DSA feedback.

The flux distribution of the accelerated OpenMC agrees the reference fluxes well at 1,000th cycle and demonstrates that the OpenMC calculation converges correctly with the DSA feedback turned on. However, a closer look at how the flux distribution changes as the iterations advance show that the DSA feedback introduces an "overshoot" in flux distribution towards a higher multiplication, i.e., the flux is more concentrated towards the center of the slab. Although this overshoot dies away with the iterations, and is barely present at 500th cycle, it still slows down the source convergence in the hybrid method.

In order to better illustrate process of source convergence, the Shannon entropy of the corrected flux distribution is calculated using the same spatial mesh at each cycle, shown in Fig. B.2. Starting from a uniform distribution, the DSA corrected fluxes first transform quickly towards convergence in shape, overshoots and then come back to the correct shape around Cycle 350-400. This is consistent with the flux shape in Fig. B.1. If we consider the source convergence is achieved at the 400th cycle, the speedup is approximately 3.5.

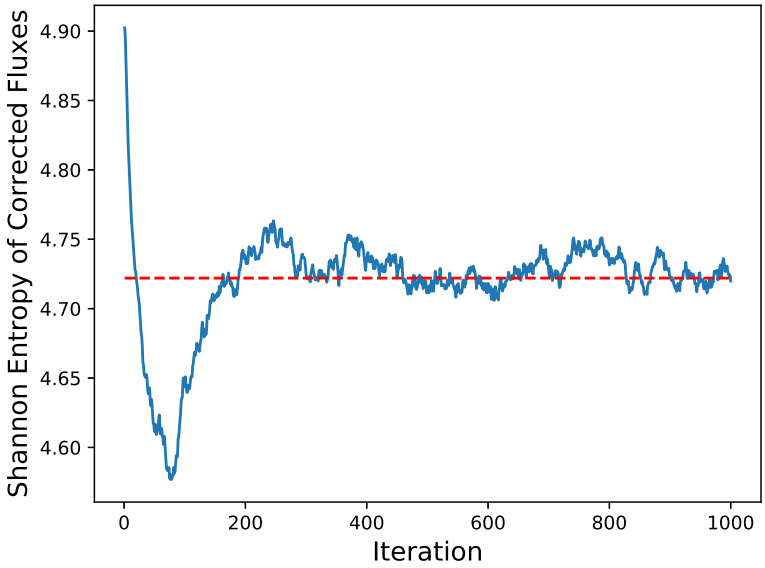

Figure B.2: Shannon entropy of corrected flux versus iteration.

To avoid the overshoot, the DSA feedback has to be turned off at certain point. As shown in Fig. B.2, the hybrid method first reaches convergence around Cycle 50-60. In the next case the DSA feedback is turned off at 55th cycle and the flux shape is checked at different cycles, shown in Fig. B.3. In this case the source distribution convergences around 200th cycle and the Shannon entropy shown in Fig. B.4 confirms this. With the DSA feedback turned off at earlier stage, the convergence has been accelerated by a factor of 7.

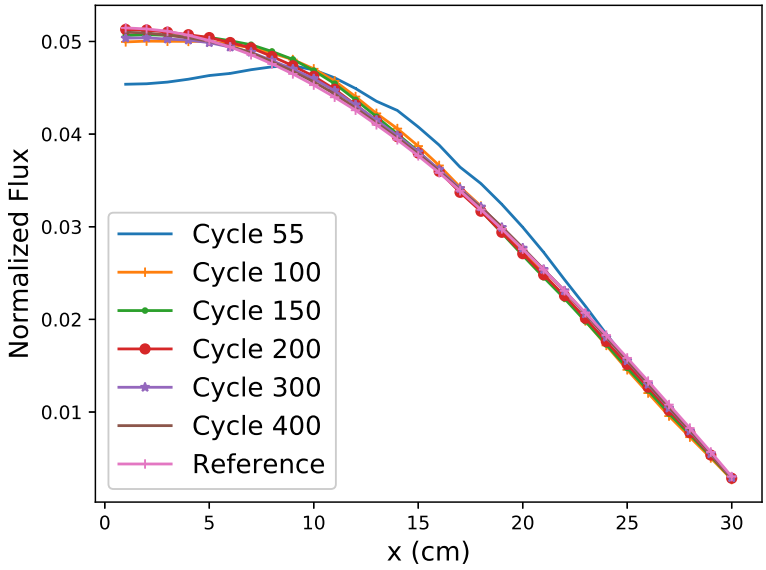

Figure B.3: Normalized flux at different cycles with DSA turned off at 55th cycle.

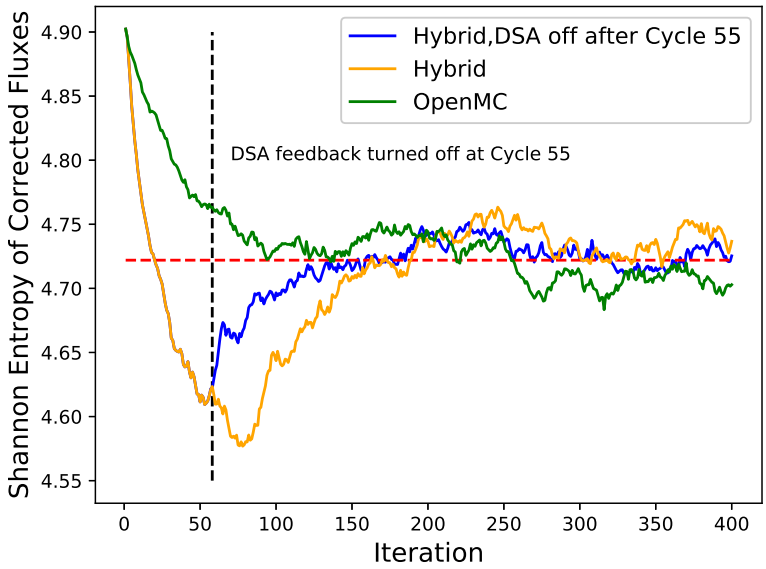

Figure B.4: Shannon entropy of corrected flux versus iteration with DSA turned off at 55th cycle.

The performance of MC-DSA is unsatisfying in two aspects:

- The convergence stability is not optimal even for simple case like this homogeneous slab. In comparison, DSA in S_N calculations was proven to be unconditionally stable if consistently discretized. Though the consistency between Monte Carlo calculation and DSA is unclear and not established, the impact on its convergence stablity is rather disappointing.

- Acceleration in source convergence process relies on manual manipulation. This behavior is similar to that of FDSA, and when to turn off the DSA feedback is also entirely empirical. For the purpose of hybrid method, an automatic global acceleration is what the method should aim for.

These results led us to believe that linear DSA is not an adequate candicate for the development of hybrid method and the inclusion of nonlinear fission synthetic operator would be a better approach to design a low-order problem for the acceleration of power iteration method.

B.2 Mesh-refinment study on S_N solver

In the development of one-group FDSA method in S_N solver, we conducted a mesh refinement study to test the convergence rate and more importantly the validation of the method.

While we were trying to determine the proper formulation of FDSA, two schemes were investigated. The FDSA-I is as presented in Chapter 2, while low-order FDSA-II problem is slightly different on the right hand side

$$-\frac{\partial}{\partial x}\frac{1}{3\Sigma_{t,g}}\frac{\partial}{\partial x}f_{0,g}^{(l+1)}+\Sigma_{t,g}f_{0,g}^{(l+1)}-\sum_{g'=1}^{G}\Sigma_{s,g'\to g}f_{0,g'}^{(l+1)}-\frac{\chi_g}{k^{(l+1/2)}}\sum_{g'=1}^{G}\nu_{f,g'}\Sigma_{f,g'}f_{0,g'}^{(l+1)}=$$
$$\frac{\chi_g}{k^{(l+1/2)}}\sum_{g'=1}^{G}\nu_{f,g'}\Sigma_{f,g'}\phi_{g'}^{(l+1/2)}-\frac{\chi_g}{k^{(l)}}\sum_{g'=1}^{G}\nu_{f,g'}\Sigma_{f,g'}\phi_{g'}^{(l)}$$
$$+\sum_{g'=1}^{G}\Sigma_{s,g'\to g}\phi_{g'}^{(l+1)}-\sum_{g'=1}^{G}\Sigma_{s,g'\to g}\phi_{g'}^{(l)}\ , \quad \text{(B.1)}$$

to include the difference of scattering sources from the transport solution.

With the combination of DSA and FDSA, we had a few acceleration modes for comparison purposes, and these modes were:

1. Mode 0: S_N transport sweep, no acceleration
2. Mode 1: S_N+DSA
3. Mode 2: S_N+FDSA-I
4. Mode 3: S_N+DSA+FDSA-I
5. Mode 4: S_N+FDSA-II
6. Mode 5: S_N+DSA+FDSA-II

7. Mode 6: S_N+CMFD

The difference of which is whether to include the scattering synthetic operator on the right hand side of FDSA equation A.14. Later it was found out that if the scattering synthetic operator is included, FDSA-II would provide over-correction that severely impacts the convergence stability in cases where the inner iteration converges the scattering source relatively fast. Hence, the FDSA-II scheme was disgarded. In the hindsight of the success on FDSA, it might be meaningful to investigate this.

Moreover, we found that the FDSA method, which functions between power iterations, can be used in conjunction with DSA, or intuitively perhaps any acceleration method applied in inner iteration, and achieve even better convergence rate. This is another point of interest that could be followed up in future development.

B.2.1 Mesh refinement with homogeneous slab

The eigenvalue calculated in the homogeneous case is gathered and compared for all cases, shown in Table B.1. Here the cross section data is $\Sigma_t = 1.0, \Sigma_s = 0.5, \nu\Sigma_f = 0.375$.

Table B.1: Eigenvalues in mesh refinement study on homogeneous slab

	Number of meshes per cell					
Mode	1	2	4	8	16	32
0	1.428151071	1.428708281	1.428848223	1.42888315	1.428891877	1.428894059
1	1.428151071	1.428708281	1.428848223	1.428883149	1.428891877	1.428894059
2	1.428151079	1.428708281	1.428848222	1.428883149	1.428891877	1.428894059
3	1.428151074	1.428708291	1.428848233	1.428883151	1.428891879	1.428894061
4	1.428151078	1.428708289	1.428848224	1.428883151	1.428891879	1.428894061
5	1.428151061	1.428708292	1.428848234	1.428883161	1.428891889	1.42889407
6	1.42815108	1.428708291	1.428848232	1.428883159	1.428891887	1.428894068

If the S_N solution with the finest mesh in red is regarded as reference solution and used to calculate the error, the mesh refinement results are shown in Fig. B.5. Judging from this, the solvers implemented so far are rather consistent in convergence behavior, at least for this specific case. The rate of convergence in these schemes are second order. For cases with different scattering ratios the DSA+FDSA-II solver do not converge correctly hence we chose FDSA-I as the final form of low-order FDSA problem.

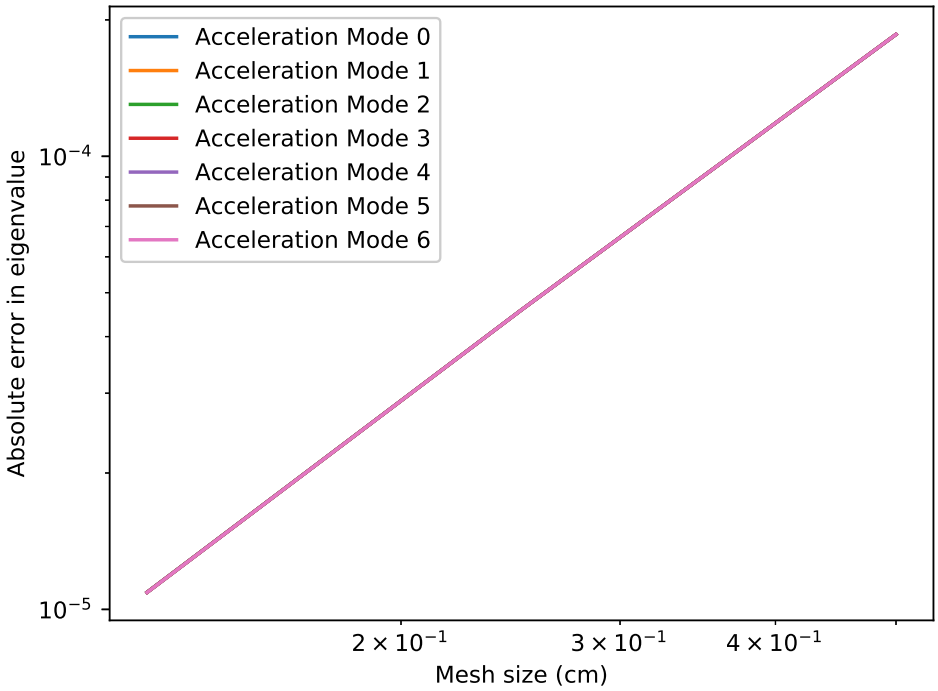

Figure B.5: Error in eigenvalue versus mesh size for different solvers

The number of iterations consumed by each solver for the above mesh refinement study is shown in Table B.2. This is what we expected for Mode 0-5. Since the CMFD solver, Mode 6, is not converging to the correct solution, we are not sure how the FDSA schemes are compared to CMFD performance wise.

Table B.2: Number of transport sweep for all modes in mesh refinement study on homogeneous slab

	Number of meshes per cell					
Mode	1	2	4	8	16	32
0	88	94	96	96	96	96
1	49	52	53	53	53	53
2	50	47	47	47	47	47
3	26	29	29	26	26	26
4	49	55	52	52	52	52
5	20	24	24	24	24	24
6	48	52	53	53	53	53

B.2.2 Mesh refinement with heterogeneous slab

We also have the mesh refinement results on the heterogeneous case, with the eigenvalues in Table B.3 and the number of iterations in Table B.4.

Table B.3: Eigenvalues in mesh refinement study on heterogeneous slab

	Numer of meshes per cell					
Mode	1	2	4	8	16	32
0	0.543601	0.590257	0.596694	0.598525	0.598998	0.599115
1	0.543601	0.590257	0.596694	0.598525	0.598998	0.599115
2	0.543601	0.590257	0.596694	0.598525	0.598998	0.599115
3	0.543601	0.590257	0.596694	0.598525	0.598998	0.599115
4	0.543601	0.590257	0.596694	0.598525	0.598998	0.599115
5	0.543601	0.590257	0.596694	0.598525	0.598998	0.599115
6	0.543601	0.590257	0.596694	0.598525	0.598998	0.599115

Table B.4: Number of transport sweep for all modes in mesh refinement study on heterogeneous slab

	Numer of meshes per cell					
Mode	1	2	4	8	16	32
0	3395	2367	2341	2335	2334	2333
1	1654	1094	1071	1066	1064	1064
2	553	348	310	304	304	303
3	268	160	141	138	137	137
4	268	159	141	139	138	138
5	128	72	62	61	61	61
6	1587	1036	995	990	988	989

And we have the error in eigenvalue versus the mesh size plot in Fig. B.6. These results indicate that all the solvers have been implemented correctly. In the aspect of performance, FDSA-II outperforms CMFD in both tests, however, keep in mind that the low-order problem needs to be eigenvalue themselves to achieve the best performance.

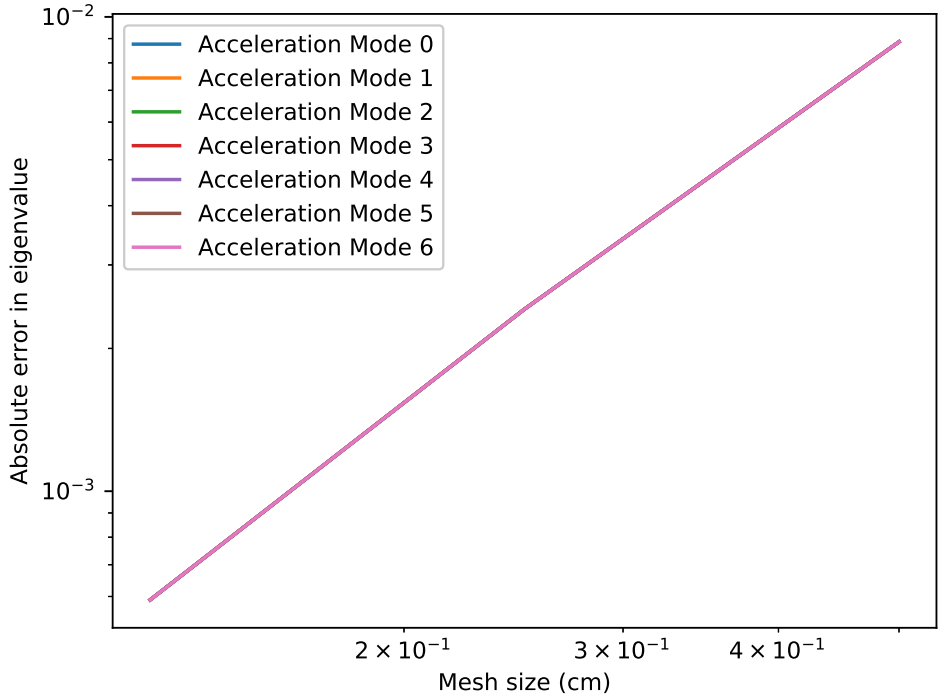

Figure B.6: Error in eigenvalue versus mesh size for different solvers

The mesh refinement study on FDSA confirms that the novel FDSA method performs well on convergence stability numerically. All calculation modes satisfy a first-order accuracy as expected. The success of this part of study helps us advance the development process to the multigroup FDSA method.

B.3 S_N tests on FDSA

B.3.1 One-group heterogeneous slab with hot fuel

This is one of the tests in which FDSA by Urbastch failed to converge without damping. Its geometry is exactly the same as the uniform lattice case featured in Chapter-3, Section 3.1.1, except that the fuel cell next to the reflective boundary is replaced with a hot fuel cell with larger fission cross section. The cross section of the three materials are:

1. Cross section of Fuel: $\Sigma_t = 1.0, \Sigma_s = 0.7, \nu\Sigma_f = 0.3071$
2. Cross section of Hot fuel: $\Sigma_t = 1.0, \Sigma_s = 0.7, \nu\Sigma_f = 0.4071$
3. Cross section of Absorber: $\Sigma_t = 1.0, \Sigma_s = 0.001, \nu\Sigma_f = 0.0$

This makes the test more difficult as the gradient of flux near the hot fuel is extremely high, and thus the solution is very un-diffusion-like. The eigenvalues and number of iterations consumed by FDSA and CMFD are gathered in Table B.5.

Table B.5: Eigenvalues and number of transport sweeps in heterogeneous slab with hot fuel test

	Eigenvalue	No. of transport sweeps
SN	0.723997533	227
SN+FDSA	0.723997535	50
SN+DSA+FDSA	0.723997551	23
SN+CMFD	0.723997538	12

Though other metrics might be used to illustrate the convergence process, the novel FDSA method has good convergence stability compared to the original FDSA method. The convergence

process in FDSA does not require damping and would converge to correct solution for extreme cases like this.